EBF2 variant identified in a patient with atypical partial lipodystrophy causes adipose fibrosis and dysfunction

Maria C. Foss-Freitas[1*], Donatella Gilio[1,2*], Lynn Pais[3,4], Eric D. Buras [1], Romil Kaul Verma [1], Melanie O'Leary[4], Heidi L. Rehm[4], Carmen Glaze[4], Kathryn Russell[4], Andre Monteiro da Rocha[5], Adam Neidert[1], Patrick Seale[6], Miriam S. Udler[4], Elif A. Oral[1†], Tae-Hwa Chun[1,7†]

1. Caswell Diabetes Institute and Metabolism, Endocrinology and Diabetes Division, Department of Internal Medicine, University of Michigan Medical School, Ann Arbor, Michigan, USA.
2. Department of Clinical and Translational Sciences, University of Pisa, Pisa, Italy.
3. Division of Genetics and Genomics, Boston Children's Hospital, Boston, USA.
4. Broad Institute Center for Mendelian Genomics and Program in Medical and Population Genetics, Broad Institute of MIT and Harvard, Cambridge, USA.
5. Frankel Cardiovascular Regeneration Core Laboratory, University of Michigan, Ann Arbor, Michigan.
6. Institute for Diabetes, Obesity & Metabolism, Department of Cell and Developmental Biology, Perelman School of Medicine at the University of Pennsylvania, Philadelphia, USA.
7. Biointerfaces Institute, The University of Michigan, Ann Arbor, Michigan, USA.

*Shared first-authorship

†Shared senior-authorship and co-corresponding authors:

eliforal@med.umich.edu (E.A.O.), taehwa@umich.edu (T.H.C.)

2800 Plymouth Rd, Ann Arbor, MI 48109

Conflicts of interest

MFF, DG, RKV, AMR, AN, LP, EDB, MO, HLR, CG, KR, PS, MSU, and THC declare no competing interests. EAO consults for and receives support for clinical trials and grants from Amryt (Chiesi), Regeneron, and Ionis; consults with Third Rock Ventures (Marea Therapeutics) and Rejuvenate Inc.; and received grant support from PTC Therapeutics within the past two years. She holds IP rights to metreleptin (Amryt/Chiesi) and is entitled to royalties. She also has ongoing trial support from Novo Nordisk, Rhythm Pharmaceuticals, and Morphic Medical (formerly GI Dynamics), unrelated to lipodystrophy.

Abstract

Lipodystrophy syndromes are characterized by loss of adipose tissue (AT), leading to insulin resistance and the development of metabolic syndrome. We identified a heterozygous nonsense variant in early B cell factor 2 (*EBF2*) (Chr8:26033143C>A, NM_022659.4: c.493G>T, p.E165X) in a patient with atypical partial lipodystrophy (PLD). The EBF family is crucial for the differentiation and function of various mesenchymal tissues. Through in vitro and in vivo disease models, we discovered that this variant limits adipocyte differentiation and hampers adipose tissue remodeling. Heterozygous knock-in ($Ebf2^{E165X/+}$) mice showed restricted adipogenesis and defective extracellular matrix (ECM) remodeling during post-weaning and high-fat diet (HFD)-induced adipose tissue expansion. HFD caused abnormal adipocyte hypertrophy, decreased expression of adiponectin and leptin, and glucose intolerance in $Ebf2^{E165X/+}$ mice. Furthermore, key mitochondrial genes involved in fatty acid metabolism and oxidation were downregulated specifically in $Ebf2^{E165X/+}$ adipose tissue. Our results suggest that EBF2 dysfunction driven by this nonsense variant drives disease pathology, establishing a connection between EBF2 disruption and an atypical form of lipodystrophy.

Introduction

Lipodystrophy syndromes (LD) are characterized by loss of adipose tissue (AT), leading to insulin resistance and metabolic dysfunction (1-3). These diseases present with generalized or partial fat loss (3, 4). The genetic underpinnings of about 30% of generalized lipodystrophy and 50% of partial lipodystrophy (PLD) syndromes remain unsolved (2). To better define the molecular basis of PLD, we initiated the genetic investigation of affected individuals using whole-genome sequencing. As part of these efforts, we evaluated a young patient with peripheral AT loss with extensive fibrosis, steatohepatitis, nephrosclerosis, insulin resistance, and dyslipidemia (5, 6). Initial genetic screening did not identify causative variants in known lipodystrophy genes (5). We then performed whole-genome sequencing. By filtering for disruptive gene variants and cross-referencing with clinical databases, we identified a nonsense variant of *EBF2* (8:26033143C>A, c.493G>T, p.E165X).

EBF2 is a member of the early B-cell factor (*EBF*) family, also referred to as Olf-1/EBF (O/E) or Collier/Olf-1/EBF (COE) (7), which plays a crucial role in the differentiation of multiple cell lineages (8-14). The *EBF* family promotes adipocyte differentiation (8), and reduced *EBF1* expression is linked to limited adipocyte hyperplasia, adipocyte hypertrophy, and insulin resistance in humans (15). *Ebf2* regulates mouse brown adipocyte fate in concert with *Pparg* (16). In white AT (WAT), *Zfp423* antagonizes *Ebf2* to suppress the thermogenic program (17). In addition, *EBF2* is enriched in a subset of human visceral adipocytes and linked to increased waist-hip ratio (18). Moreover, genome-wide association studies (GWAS) identified *EBF2* variants associated with hypertension (19), diabetic nephropathy, and visceral adipose mass (20).

Based on these findings, we hypothesized that the *EBF2* stop-gain variant (p.E165X) identified in this patient could cause PLD. The truncated variant, EBF2 (1-164), suppressed adipocyte differentiation in 3T3-L1 cells that express endogenous *Ebf1*, *Ebf2*, and *Ebf3* (8), raising the possibility that EBF2 (1-164) acts as a dominant-negative inhibitor of adipogenesis. However, in vitro adipogenesis may differ from in vivo processes, which are influenced by humoral factors (21), the three-dimensional structure of tissues (22), and oxygenation status (23, 24). Further, adipose tissue development involves mesenchymal cell proliferation, adipocyte differentiation (25-27), extracellular matrix (ECM) remodeling (22), and angiogenesis (28). In addition, adipose tissue development and expansion processes vary across perinatal, postnatal, and adult stages and differ between fat depots (29, 30), with distinct transcriptional networks governing adipose tissue development and function (25-27). To investigate the pathological effects of the *EBF2* nonsense variant on AT development, we generated a knock-in (KI) mouse model carrying the single-nucleotide change identified in our patient ($Ebf2^{E165X/+}$). The $Ebf2^{E165X/+}$ mice exhibited restricted adipogenesis and impaired ECM remodeling, resulting in AT dysfunction and the persistent presence of a collagen-rich ECM, similar to what we observed in our patient. Using primary mouse preadipocytes, we found that the *EBF2* p.E165X variant causes cell-autonomous defects in adipocyte differentiation and maturation. These findings demonstrate that EBF2 dysfunction disrupts adipose tissue development and function.

Results

Case presentation

The patient is a 23-year-old female with PLD (Figure 1, A and B) who first presented to medical attention at age 9 with hypertriglyceridemia and hepatomegaly. She was referred to us at age 11 when AT loss affecting the hips and legs was noted. Although her complex clinical presentation has been previously reported (5, 6), it is worthwhile to review key clinical details. She was born as one of a pair of fraternal twins, conceived through in vitro fertilization by her 38-year-old parents. Her father, diagnosed with atypical lupus, type 2 diabetes, and heart failure, died from sudden cardiac arrest on the night of the embryo transfer. She and her fraternal twin were born to her mother at 38 weeks of pregnancy after an uneventful pregnancy, other than the trauma of her father's unexpected death. She was observed to have an umbilical hernia and contracture of the fifth digit of the right hand. She showed no neurodevelopmental delays and achieved all developmental milestones without issues. Additionally, she displayed normal baby fat during her first year of life. Hepatomegaly was detected at age 8.5. Labs done in that year demonstrated hypertriglyceridemia and elevated liver enzymes. Her pediatrician also noted scoliosis. She was referred to our clinic after a local endocrinologist noted fat loss in her extremities and prominent veins. During the interview, the patient and her mother reported that an unusual fat distribution in the legs was noticed as early as age 6 when she began playing soccer, and her teammates commented on her leg appearance. In our initial evaluation at age 11, the clinical examination revealed signs of partial lipodystrophy, characterized by fat loss in the lower limbs, with palpable adipose tissue in the abdomen and increased fat deposits around the face, neck, and upper trunk. The liver was enlarged, with a total liver span of 17 cm, and the abdomen was protuberant. She had no palpable breast tissue and no signs of puberty. No lipodystrophy phenotype was observed in her fraternal twin brother, older sister, or mother. Labs demonstrated hypertriglyceridemia, insulin resistance, and prediabetes. Additional lab findings included low-titer anti-GAD antibodies, low complement C4 levels, elevated liver transaminases, and massive proteinuria. In the next decade, she developed primary hypogonadotropic hypogonadism, clinically complicated diabetes, and hypertriglyceridemia (5, 6). Also, progressive elevations in liver enzymes and worsening proteinuria were observed, prompting liver and kidney biopsies. Histological examination of the liver showed hepatocyte ballooning with excess lipid accumulation and fibrosis (Figure 1C); the kidney demonstrated fibrotic ECM accumulation in the glomerulus and interstitium, described by the case pathologist as "Alport-like pathology" (Figure 1C). Biopsies of subcutaneous adipose tissue depots (abdomen, neck, and thigh) showed abnormal architecture, with accumulated ECM replacing adipocytes (Figure 1C).

Molecular investigations identified a nonsense variant in *EBF2* (p.E165X) as potentially pathogenic

We attempted to uncover the molecular basis of presentation in our patient. First, a lipodystrophy gene panel (*AGPAT2, AKT2, BSCL2, CAV1, CIDEC, LMNA, PLIN1, PPARG, PTRF, TBC1D4,* and *ZMPSTE24*) (5) detected no known or unknown variants. Subsequently, we performed whole-exome sequencing (WES) with blood samples of the proband, mother, and two siblings. A detailed list of unique variants is available in Supplemental Table 1. Two protein-truncating rare variants (*LEKR1 p.G123X* and *EBF2 p.E165X*) were among the heterozygous variants not shared by her family members. Our research laboratory reported these two variants as genetic variants of unknown significance. To gather confirmatory evidence and ensure that no other genomic findings explain the patient's clinical phenotype, we contacted the Broad Institute to undertake whole-genome analyses of the proband and her mother. The variant call set was uploaded to *seqr* (31) for collaborative study, and then the Broad Institute Center for Mendelian Genomics (CMG) performed variant filtration searches (31) based on suspected mode of inheritance, pathogenicity reported in ClinVar, type of variant, frequency in population databases, and variant call quality.

We assessed candidate variants for genotypic and phenotypic concordance with known disease genes using Online Mendelian Inheritance in Man (OMIM) and a targeted literature review. As no candidates were identified in known disease genes, we screened high-impact variants in genes of uncertain significance (GUS). Among them, we identified a stop-gain variant in *EBF2*, which was also noted in our prior WES (Supplemental Figure 1A). This *EBF2* variant was confirmed with targeted Sanger sequencing (Figure 1D). The heterozygous nonsense variant of *EBF2* (NM_022659.4) was found in exon 6, leading to the premature termination of EBF2 at amino acid position 165 (chr8:26033143 C>A, *EBF2* c.493G>T, p.E165X). Genomic DNA was then isolated from her father's hair collected from his hairbrush. Whole-genome sequencing demonstrated the identical *EBF2* variant (chr8:26033143 C>A), thereby confirming paternal inheritance (Supplemental Figure 1B).

There is substantial evidence linking *EBF2* to a lipodystrophy-like phenotype. At the gene level, the Human Genetic Evidence "HuGE" Calculator indicated "Very Strong" support for associations between *EBF2* and type 2 diabetes, body fat distribution (waist-hip ratio, visceral/gluteofemoral adipose ratio, visceral/abdominal adipose ratio, visceral adipose tissue adjusted for BMI), and cardiometabolic phenotypes (hypertension, systolic blood pressure, diastolic blood pressure, pulse pressure, HDL cholesterol, triglyceride) (CMDKP: hugeamp.org). In large-scale genome-wide association studies, the G allele of *EBF2* SNP (rs17818197) is associated with increased risk of type 2 diabetes (OR 1.02, $p = 7.69\times10^{-12}$)(31), reduced HDL cholesterol (Beta -0.0058, $p = 1.96\times10^{-6}$) (32), increased systolic blood pressure (Beta 0.0082, $p = 2.8\times10^{-6}$) (HuGEAMP), increased risk of hypertension (OR 1.02, $p = 4.5\times10^{-7}$) (33), and increased triglyceride levels (Beta 0.0061, $p = 1.67\times10^{-5}$) (32). This phenotypic pattern aligns with a lipodystrophy-like clinical presentation (34, 35). Additionally, rare variant burden testing for *EBF2* in 344,692 individuals identified an association of 198 predicted deleterious missense and loss-of-function (LoF) variants in *EBF2* with increased random glucose levels (p=0.0028) (36).

EBF2 is highly constrained for protein-truncating variation in the general population, with a probability of loss-of-function Intolerance (pLI) score of 1.0 and an observed/expected (o/e) LoF ratio of 0.26 (37, 38). We manually reviewed the LoF variants in gnomAD (Supplemental Table 2) using the advanced variant classification framework (37). Out of 57 predicted LoF (pLoF) variants, 25 of them (44%) are not expected to result in protein truncation for a variety of reasons, including in-frame splicing (N=7), termination in the last exon or last 50 bp of penultimate exon (N=8), genotyping error (N=1), and presence in a non-biologically relevant transcript (N=9). Of the remaining 32 variants predicted to result in LoF, 5 are present in gnomAD v3.1.2. As gnomAD v4 includes samples from biobanks and disease-specific studies, and v3.1.2 has controls from cardiovascular and diabetes cohorts, some individuals may display symptoms of lipodystrophy. Based on these findings, we considered the *EBF2* stop-gain variant identified in this patient to be potentially causative of the patient's PLD-related metabolic phenotype.

EBF2* p.E165X variant impairs adipogenesis *in vitro

We have utilized 3T3-L1 adipocyte differentiation for the initial functional screening of candidate gene variants identified in our patients with lipodystrophy syndromes. *Ebf2* knockdown in 3T3-L1 preadipocytes using two independent siRNA oligonucleotides (Supplemental Figure 2, A-C and Supplemental Table 3) reduced lipid accumulation and decreased the expression of adipocyte genes, *Pparg* and *Fabp4* (Supplemental Figure 2, A and C). To assess the activity of the identified *EBF2* variant, we used lentiviral vectors to express full-length and truncated variant (1-164) forms of *EBF2* in 3T3-L1 preadipocytes following silencing endogenous mouse *Ebf2*. We used five different lentiviral shRNA constructs to stably knock down *Ebf2* (Supplemental Table 4) and chose a clone (clone-4) that showed specific suppression of *Ebf2* relative to *Ebf1*. As expected, these cells showed low levels of adipocyte differentiation (Figure 1E). Full-length *EBF2* restored robust adipogenesis (Figure 1E), whereas the variant *EBF2* (1-164) did not (Figure 1E), supporting the loss of function for the *EBF2* (1-164) variant. Consistent with this, the truncated EBF2 variant failed to activate transcription from an EBF2-driven reporter gene (Figure 1F). Together, these results suggest that the truncated EBF2 variant is a LoF mutation.

EBF2 p.E165X variant impairs postnatal adipose tissue expansion and remodeling in vivo

Based on the in vitro results, we hypothesized that the truncated *EBF2* variant may have caused adipose tissue loss in our patient. To test this hypothesis in vivo, we generated a KI mouse model harboring the observed nonsense variant ($Ebf2^{E165X/+}$) using CRISPR/Cas9 genome editing (39). While we had no difficulty obtaining heterozygous KI mice, we rarely obtained surviving homozygous mice ($Ebf2^{E165X/E165X}$) on the C57BL/6J background. However, a few $Ebf2^{E165X/E165X}$ mice were successfully weaned on a mixed genetic background. A surviving female $Ebf2^{E165X/E165X}$ mouse lacked perigonadal white adipose tissue (WAT) and showed rudimentary subcutaneous and inguinal WAT with dysmorphic adipocytes and extensive accumulation of eosinophilic fibrillar structures (Supplemental Figure 2D). The WAT displayed extensive fibrosis, characterized by a limited number of adipocytes surrounded by excess ECM proteins (Supplemental Figure 2, D-F). Unlike homozygous KI mice, $Ebf2^{E165X/+}$ mice were born without noticeable defects, and there was no difference in weight between $Ebf2^{+/+}$ and $Ebf2^{E165X/+}$ mice at eight weeks of age (Supplemental Figure 3A). $Ebf2^{+/+}$ and $Ebf2^{E165X/+}$ showed comparable weight gain (Supplemental Figure 3B) and food intake (Supplemental Figure 3C) during an additional 8 weeks of chow diet (CD) feeding. Moreover, $Ebf2^{+/+}$ and $Ebf2^{E165X/+}$ mice displayed similar body composition as assessed with NMR-based analysis, % inguinal, gonadal white adipose tissue, and brown adipose tissue (IWAT, GWAT, BAT) mass, and liver weights (Supplemental Figure 3, D-F). Fasting serum glucose levels were not different between the groups (Supplemental Figure 3G), but insulin levels were higher in male $Ebf2^{E165X/+}$ compared to $Ebf2^{+/+}$ mice (Supplemental Figure 3H). Plasma glucose levels during the intraperitoneal glucose tolerance test (IPGTT) were similar between the groups (Supplemental Figure 3I); however, fasting serum triglyceride levels were elevated in male

Ebf2$^{E165X/+}$ mice (Supplemental Figure 3J). The livers showed no histological differences between the groups (Supplemental Figure 3K).

We next evaluated the histological features of WAT from *Ebf2*$^{+/+}$ and *Ebf2*$^{E165X/+}$ mice. Hematoxylin and Eosin (H&E) staining of IWAT revealed the heterogeneity of adipocyte size in *Ebf2*$^{E165X/+}$ mice (Figure 2A). Notably, smaller adipocytes were typically surrounded by clusters of stromal cells (Figure 2A). *Ebf2*$^{E165X/+}$ IWAT also displayed groups of adipocytes surrounded by thick collagen fibrils stained blue with Masson's trichrome (MT) staining (Figure 2A). In GWAT, we observed less heterogeneity in adipocyte size (Figure 2B). However, the clusters of stromal cells were found preferentially in *Ebf2*$^{E165X/+}$ mice (Figure 2B). These stromal cell clusters were often found adjacent to collagenous materials stained blue with MT staining (Figure 2B). Quantification of IWAT fibrosis based on trichrome-positive area showed increased fibrosis in tissues from *Ebf2*$^{E165X/+}$ relative to *Ebf2*$^{+/+}$ controls (Figure 2C). Given the alterations in adipose tissue structure, we also analyzed the expression of key adipocyte genes in WAT depots of *Ebf2*$^{+/+}$ and *Ebf2*$^{E165X/+}$ mice. *Adipoq* and *Lpl* were reduced in IWAT (Figure 2D). *Lep* was also decreased in male *Ebf2*$^{E165X/+}$ mice (Figure 2D). The two genotypes showed equivalent expression of these adipocyte genes in GWAT (Supplemental Figure 3L), suggesting that IWAT structure and function are selectively impacted in *Ebf2*$^{E165X/+}$ mice.

To further investigate when the differences in IWAT structure between *Ebf2*$^{+/+}$ and *Ebf2*$^{E165X/+}$ mice manifest, we analyzed IWAT at 4 and 16 weeks of age. Notably, at 4 weeks, there was no substantial difference in IWAT structure between *Ebf2*$^{+/+}$ and *Ebf2*$^{\mathrm{E165X/+}}$ mice. In both groups, IWAT exhibited adipocytes of varying sizes and discrete regions of intense eosin staining (Supplemental Figure 4A); closer examination revealed clusters of smaller adipocytes (Supplemental Figure 4A). MT staining showed the persistent presence of thick collagen fibrils and the reminiscence of the primordial mesenchyme (Supplemental Figure 4B). Despite the accumulation of collagenous materials in *Ebf2*$^{E165X/+}$ mice, *Col1a1* transcript levels were downregulated, indicating that collagen persistence likely reflects impaired ECM remodeling rather than increased synthesis (Supplemental Figure 4C). Immunofluorescent staining demonstrated the presence of fibronectin, type I and VI collagens adjacent to CD34^{+} cells (Figure 2E, Supplemental Figure 4, D-, F, G). IWAT from 16-week-old *Ebf2*$^{+/+}$ mice displayed a reduction in ECM proteins (collagens and fibronectin), as well as a decrease in the number of CD34^{+} cells, compared to the 4-week-old *Ebf2*$^{+/+}$ mice (Figure 2E, Supplemental Figure 4, D-I). By contrast, IWAT from 16-week-old *Ebf2*$^{\mathrm{E165X/+}}$ mice, both male and female, displayed excess ECM deposits enmeshed with CD34+ cells (Figure 2E, Supplemental Figure 4D-E). The persistence of CD34^{+} cells surrounded by ECM deposits in *Ebf2*$^{E165X/+}$ mice suggests a critical role for *Ebf2* in coordinating ECM remodeling and adipocyte maturation, biological processes essential for adipose tissue expansion between 4 and 16 weeks of age.

EBF2 **p.E165X variant disrupts high-fat diet-induced adipose tissue remodeling and expansion**

To determine whether diet interacts with the presence of the *Ebf2* variant, we challenged a group of *Ebf2*$^{+/+}$ and *Ebf2*$^{E165X/+}$ mice with a 45% kcal high-fat diet (HFD) for two months, starting at eight weeks of age. A few months of HFD challenge is sufficient to induce adipose tissue remodeling (30-33). *Ebf2*$^{+/+}$ and *Ebf2*$^{E165X/+}$ mice, males and females, started from the same weight (Figure 3A) and gained comparable weight after 8 weeks of HFD (Figure 3B) with similar food intake (Figure 3C). Although *Ebf2*$^{+/+}$ and *Ebf2*$^{E165X/+}$ mice gained the same weight, NMR-based body composition analysis showed reduced % fat (lipid) mass and higher % lean mass in female *Ebf2*$^{E165X/+}$ compared to *Ebf2*$^{+/+}$ mice (Figure 3, D and E). HFD increased serum leptin levels in both *Ebf2*$^{+/+}$ and *Ebf2*$^{E165X/+}$ mice, but the response was attenuated in *Ebf2*$^{E165X/+}$ mice (Figure 3F).

Serum adiponectin levels were lower in *Ebf2*$^{E165X/+}$ mice than in *Ebf2*$^{+/+}$ mice (Figure 3G). However, we did not detect differences in IWAT or GWAT mass between *Ebf2*$^{+/+}$ and *Ebf2*$^{E165X/+}$ mice for both sexes, suggesting the shift of lipid to non-lipid constituents in female *Ebf2*$^{E165X/+}$ IWAT (Supplemental Figure 5A). Indeed, histological analysis revealed increased stromal cell clusters and collagen fiber accumulation in *Ebf2*$^{E165X/+}$ IWAT (Figure 3H). Additionally, GWAT from *Ebf2*$^{E165X/+}$ mice showed more infiltration of immune cells and crown-like structure than *Ebf2*$^{+/+}$ mice (Figure 3I), particularly in males, suggesting an enhanced inflammatory response in *Ebf2*$^{E165X/+}$ mice. The adipocyte area in IWAT increased in both *Ebf2*$^{+/+}$ and *Ebf2*$^{\mathrm{E165X/+}}$ mice following HFD, with hypertrophy more pronounced in *Ebf2*$^{\mathrm{E165X/+}}$ mice (Figure 3J). Adipocyte number was correspondingly lower in IWAT of *Ebf2*$^{E165X/+}$ compared to *Ebf2*$^{+/+}$ mice (Figure 3J). The quantified fibrosis index was higher in *Ebf2*$^{E165X/+}$ IWAT, but not in GWAT (Figure 3K). GWAT also showed augmented HFD-dependent adipocyte hypertrophy with decreased adipocyte number in *Ebf2*$^{E165X/+}$ male mice relative to *Ebf2*$^{+/+}$ male mice (Figure 3L**).** These findings indicate that HFD promotes adipocyte hypertrophy while limiting hyperplasia in *Ebf2*$^{\mathrm{E165X/+}}$ mice, a pattern reminiscent of the restricted adipogenesis with paradoxical hypertrophy reported in *Ebf1*-null mice (15).

At the gene expression level, *Adipoq* was decreased in IWAT and GWAT of male *Ebf2*$^{E165X/+}$ mice compared to *Ebf2*$^{+/+}$ mice (Supplemental Figure 5B). *Lpl* was also lower in IWAT of male *Ebf2*$^{E165X/+}$ mice, while no differences were observed in other adipocyte genes, such as *Pparg*, *Fabp4*, and *Lep*, when the mice were fed HFD (Supplemental Figure 5B). We did not detect gene expression changes in WAT depots between female *Ebf2*$^{+/+}$ and *Ebf2*$^{E165X/+}$ mice fed HFD (Supplemental Figure 5C). HFD did not alter the signals for type I and VI collagens in IWAT compared to the CD group in either genotype. However, *Ebf2*$^{E165X/+}$ mice continued to exhibit persistent deposition of these collagens compared to *Ebf2*$^{+/+}$ mice (Supplemental Figure 5D). In

GWAT, the signals for type I and VI collagens remained unchanged following HFD, although the type I collagen signal tended to be higher in female *Ebf2*$^{E165X/+}$ mice (Supplemental Figure 5E).

***EBF2* nonsense variant worsens HFD-associated metabolic phenotypes**

We next examined whether the *Ebf2 p.E165X* variant causes metabolic impairment in mice fed an HFD. Fasting serum glucose levels were elevated in male *Ebf2*$^{E165X/+}$ mice after 2 months of HFD compared to *Ebf2*$^{+/+}$ mice (Figure 4A). Moreover, the intraperitoneal glucose tolerance test demonstrated impaired glucose clearance in *Ebf2*$^{E165X/+}$ male mice (Figure 4, B and C). During IPGTT, insulin levels were not different among the groups (mean with SEM, at 0’, female *Ebf2*$^{+/+}$ 2.23 ± 0.41 ng/mL vs *Ebf2*$^{E165X/+}$ 2.27 ± 0.47, P=0.94, male *Ebf2*$^{+/+}$ 3.56 ± 0.47 vs *Ebf2*$^{E165X/+}$ 4.08 ± 0.49, P=0.45; at 15’, female *Ebf2*$^{+/+}$ 3.62 ± 0.83 vs *Ebf2*$^{E165X/+}$ 2.82 ± 0.54, P=0.43, male *Ebf2*$^{+/+}$ 4.67 ± 0.44 vs *Ebf2*$^{E165X/+}$ 5.09 ± 0.85, P=0.66). Insulin tolerance test further demonstrated a reduced glucose clearance in male *Ebf2*$^{E165X/+}$ mice at 15 minutes; however, no significant difference between the groups was observed at 30 minutes in either sex (Supplemental Figure 6A). These results indicate a subtle but significantly reduced insulin-dependent glucose clearance in *Ebf2*$^{E165X/+}$ male mice. The liver showed increased steatosis in *Ebf2*$^{E165X/+}$ mice relative to *Ebf2*$^{+/+}$ mice in both sexes (Figure 4D). We wondered whether the *Ebf2*$^{E165X/+}$ metabolic phenotype was associated with lower energy expenditure, since *Ebf2* regulates brown adipose tissue (BAT) development and function (16, 34). *Ucp1* expression in BAT was affected by both genotype and diet in female mice (two-way ANOVA, P = 0.045 and 0.035, respectively) but showed no effects in male mice (P = 0.95 and 0.08). *Cidea* expression was regulated by diet but not genotype in both sexes (females, P = 0.04 and 0.35; males, P = 0.01 and 0.68) (Supplemental Figure 6B). BAT mass did not differ between *Ebf2*$^{+/+}$ and *Ebf2*$^{E165X/+}$ mice fed CD (Figure 4E), but HFD significantly increased BAT mass in male *Ebf2*$^{E165X/+}$ mice (Figure 4E). *Ebf2*$^{E165X/+}$ mice showed increased lipid droplets in BAT (Supplemental Figure 6C). This difference was further exacerbated by HFD (Supplemental Figure 6C). We observed no differences in VCO_2, VO_2, respiratory exchange ratio, and energy expenditure between the genotypes at three different temperatures: room (22°C), thermoneutral (30°C), and cold (10°C) when analyzed with either Student's t-test after normalizing for lean mass (Supplemental Figure 7, A-C) or regression analysis using lean mass as a covariate (Supplemental Figure 7, D and E). *Ebf2*$^{+/+}$ and *Ebf2*$^{E165X/+}$ mice exhibited the expected increase in energy expenditure at 10°C, confirming their similar preservation of thermogenic capacity. EBF family members may have unique and compensatory roles in regulating depot–specific adipose functions. Tissue distribution analysis showed that *Ebf1* and *Ebf2* exhibited sex- and depot-dependent expression ($p = 0.0013$ and 0.0096, respectively), while *Ebf3* expression was not depot-dependent ($p = 0.62$) (Figure 4, F and G). In *Ebf2*$^{E165X/+}$ mice, the depot-dependent expression of *Ebf1* and *Ebf2* seen in females was absent, indicating that the *Ebf2* variant negatively impacts sex- and depot-dependent *Ebf1/2* expression (Figure 4F). In male mice, *Ebf1* and *Ebf2* are more highly expressed in GWAT, as in females, but the differences are less noticeable. *Ebf2* expression in the liver was very low in both males and females (Figure 4, F and G).

The *EBF2* variant impairs adipose tissue identity

To determine the impact of the *Ebf2* nonsense variant on WAT, we used unbiased transcriptome analyses of IWAT isolated from 4-week-old male *Ebf2*$^{+/+}$ and *Ebf2*$^{E165X/+}$ mice, before the onset of noticeable structural and functional impairments of *Ebf2*$^{E165X/+}$ mice (GSE288829). We identified 190 transcripts differentially expressed in *Ebf2*$^{E165X/+}$ *and Ebf2*$^{+/+}$ IWAT, with an adjusted p-value below 0.05 and a log2 fold change of 1.5 or greater. Notably, *Ucp1*, *Cidea*, and *Ppara* expression were significantly downregulated in the IWAT of *Ebf2*$^{E165X/+}$ mice (Figure 5A). Conversely, immunoglobulin genes were upregulated in *Ebf2*$^{E165X/+}$ mice (Figure 5A). Pathway analysis using iPathwayGuide showed reduced expression of oxidative phosphorylation, fatty acid metabolism, and adipogenesis in *Ebf2*$^{E165X/+}$ IWAT (Figure 5B). Consistently, Gene Ontology cellular component analysis identified a reduced expression of mitochondrial genes in the *Ebf2*$^{E165X/+}$ IWAT (Figure 5B). Detailed analysis of gene expression in oxidative phosphorylation and fatty acid metabolism pathways showed the reduction of mitochondria-related genes in *Ebf2*$^{E165X/+}$ mice (Figure 5, C and D). Complementary GSEA further showed positive enrichment of pathways related to epithelial–mesenchymal transition (EMT), inflammatory response, TGF-β signaling, and PI3K–AKT–mTOR signaling (Supplemental Figure 8A). In contrast, pathways associated with adipogenesis, fatty acid metabolism, oxidative phosphorylation, and cholesterol homeostasis were negatively enriched (Supplemental Figure 8B). Given the decreased mitochondrial gene expression observed in *Ebf2*$^{E165X/+}$ mice, we assessed mitochondrial morphology using transmission electron microscopy (TEM). In *Ebf2*$^{E165X/+}$ IWAT, mitochondria were more elongated and irregularly shaped with increased variability (F test $P<0.0001$) (Figure 5, E and F). *Ebf2*$^{E165X/+}$ IWAT mitochondria frequently exhibited a loss of cristae structures compared to controls, resulting in decreased electron density (Figure 5, E and G). Moreover, *Ebf2*$^{E165X/+}$ IWAT mitochondria are positioned closer to lipid droplet membranes (Figure 5, E and H).

The *EBF2* variant impairs white adipocyte differentiation in a cell-autonomous manner

In the IWAT of *Ebf2*$^{E165X/+}$ mice, wild-type and variant *Ebf2* transcripts were equally detected with respective TaqMan probes (Figure 6A). We then asked whether cell-autonomous adipocyte defects caused the IWAT phenotype of *Ebf2*$^{E165X/+}$ mice. To address this question, we isolated the stromal vascular fraction (SVF) from IWAT depots and induced adipogenesis in vitro. *Ebf2*$^{+/+}$ SVF underwent efficient morphological differentiation into lipid-containing adipocytes (Figure 6B). On the contrary, *Ebf2*$^{E165X/+}$ SVF showed significantly impaired lipid accumulation (Figure 6, B and C). Unlike IWAT SVF, the BAT SVF of *Ebf2*$^{E165X/+}$ mice exhibited adipogenic capacity comparable to controls (Supplemental Figure 9, A and B), and BAT-specific genes, e.g., *Cidea* and *Ucp1*, were expressed equally between the groups (Supplemental Figure 9C).

Pparg and *Fabp4* were expressed comparably in *Ebf2*$^{+/+}$ and *Ebf2*$^{E165X/+}$ IWAT-derived adipocytes in vitro (Figure 6D). *Lep* was too low to be reliably assessed in the in vitro model. However, *Adipoq* and *Lpl* were significantly lower in *Ebf2*$^{E165X/+}$ adipocytes (Figure 6D). Given the involvement of other *EBF*s in adipogenesis (8), we examined whether the *Ebf2* variant affected the expression of other EBF members. *Ebf1* and *Ebf3* were expressed at similar levels in *Ebf2*$^{+/+}$ and *Ebf2*$^{E165X/+}$ IWAT-derived cells (Figure 6E). In contrast, *Ebf2* expression was induced by adipogenesis but was lower in *Ebf2*$^{E165X/+}$ cells (Figure 6E). When we expressed *EBF2 (1-164)* in *Ebf2*$^{+/+}$ IWAT-derived SVF to assess the potentially dominant-negative effect of the *EBF2* variant on adipogenesis, we observed a significant reduction in adipogenic potential (Figure 6, F and G). The adipogenesis of *Ebf2*$^{+/+}$ cells after *EBF2 (1-164)* transduction was reduced to a degree similar to that of *Ebf2*$^{E165X/+}$ mice-derived SVF (Figure 6F and Figure 6G). Furthermore, full-length EBF2 cDNA could not restore the adipogenic potential of Ebf2E165X/+ cells (Figure 6, F and G), indicating a dominant-negative mechanism rather than a loss of function, through which the EBF2 variant inhibits adipogenesis. Silencing of *Ebf2* with shRNA nullified the differences in adipocyte maturation and lipid accumulation between *Ebf2*$^{+/+}$ and *Ebf2*$^{E165X/+}$ SVFs (Figure 6, F and G), supporting the causal role of the Ebf2 gene variant in these differences. Expressing the variant *EBF2* (1-164) in *Ebf2*$^{+/+}$ cells decreased *Lpl* expression (Figure 6H), and the reduced expression could not be rescued by full-length *EBF2* in *Ebf2*$^{E165X/+}$ cells (Figure 6H). However, *Fabp4* expression was unaffected in either *Ebf2*$^{+/+}$ or *Ebf2*$^{E165X/+}$ cells (Figure 6H). These results suggest that the *EBF2* variant product, EBF2 (1-164), disrupts the expression of selective adipocyte genes.

ZNF423 and ZNF521 are multi–zinc finger transcription factors that regulate adipocyte differentiation (40, 41). ZNF423 maintains white adipocyte identity in part by antagonizing the brown fat–promoting activity of EBF2 (17, 42). We hypothesized that the truncated EBF2 variant, EBF2 (1–164), disrupts white adipocyte differentiation by interfering with other EBF family members and their co-regulators, ZNF423 and ZNF521 (17, 43). To test this, we compared full-length *EBF2* and *EBF2* (1–164) using synthetic reporters containing EBF- or ZNF-response elements (11, 44, 45). *EBF1–3* increased EBF-consensus reporter activity compared with control conditions lacking these drivers, and co-expression of wild-type or truncated *EBF2* significantly modulated reporter activity (interaction $p < 0.0001$, two-way ANOVA). Both full-length and truncated *EBF2* enhanced *EBF1*-dependent luciferase activity in a dose-dependent fashion, whereas neither construct produced a consistent effect on *EBF2*-driven reporter activity; a modest increase was observed only at the highest dose of the truncated *EBF2* variant. In the *EBF3*-driven condition, low-dose wild-type EBF2 was associated with reduced reporter activity, although this effect was not consistently observed across experimental conditions (Supplemental Fig. 10A). In ZNF423-binding element reporter assays, both full-length and truncated *EBF2* suppressed reporter activity at a higher dose. In contrast, no suppression was observed in ZNF521-consensus reporter assays at this dose (Supplemental Fig. 10B). EBF consensus element reporter activity, which ZNF423 and ZNF521 could also promote, showed greater suppression by the truncated *EBF2* than full-length *EBF2* for ZNF423-driven activity. In contrast, both full-length and the truncated EBF2 suppressed ZNF521-driven activity (Supplemental Fig. 10C). Together, these findings indicate that the *EBF2* variant does not function as a dominant-negative regulator of EBF family–dependent transcription activity in this assay system, but may differentially influence transcriptional outputs involving ZNF423- and ZNF521-associated transcriptional regulatory activities in a context-dependent manner (11, 44, 45).

Loss of H3K27Ac Binding at Key Regulatory Motifs in *Ebf2*$^{E165X/+}$ Adipocyte Precursor Cells

Adipose ECM remodeling is central to adipose tissue development (22, 46) and contributes to obesity-induced adipose dysfunction (47, 48) and the establishment of obesogenic epigenetic memory (49). A subset of adipocyte precursor cells (APCs), such as Cd45^{-}Cd31^{-}Pdgfra^{+}Cd9^{+}

stromal cells, has been implicated in adipose tissue fibrosis (50) through augmented PDGFRA-mTOR signaling (51). To determine whether the change in adipose tissue cell composition contributes to the altered adipose tissue gene expression profile in *Ebf2*$^{E165X/+}$ IWAT, we applied deconvolution analysis to the 4-week-old IWAT bulk RNA-seq data using adipose snRNA-seq data (GSE236580) (49) (Supplemental Figure 11A). This analysis revealed no significant differences in cell type proportions between *Ebf2*$^{+/+}$ and *Ebf2*$^{E165X/+}$ IWAT (Supplemental Figure 11B). Likewise, the abundance of Cd45^{-}Cd31^{-}Sca1^{+}Cd9^{+} APCs, assessed by flow cytometry, was similar between the genotypes (Supplemental Figure 11, C and D).

Given the observed cell-autonomous defect in adipogenesis and the potential dysregulation of other EBF family members and interacting zinc transcription factor activities, we hypothesized that the presence of the *EBF2* variant widely disrupts transcriptional networks and impairs the pro-adipogenic potential of adipose stromal cells. To test this, we isolated SVFs from 4-week-old female *Ebf2*$^{+/+}$ or *Ebf2*$^{E165X/+}$ mice (n=3 per group). We profiled genome-wide transcription factor (TF) motif accessibility using cleavage under targets and tagmentation (CUT&RUN) with H3K27Ac as a probe. *Ebf2*$^{+/+}$ SVFs demonstrated the enrichment of a series of TF motifs, including CCCWNGGG (EBF1/EBF2), CACGTG (BMAL1, CLOCK, NPAS2), and ACCACA (RUNX1/RUNX2) in comparison with *Ebf2*$^{E165X/+}$ SVFs (Supplemental table 5). Differential H3K27Ac binding was detected in the promoter regions of *Atg4b*, *Rarg*, *Pnp*, and *Far1* (Supplemental Table 6). *Atg4b*, a direct target of *Cebpb*, contributes to adipogenesis by regulating autophagy (52). *Rarg* functions as a nuclear receptor central to the transcriptional control of adipogenesis (53). *Pnp*, which encodes purine nucleoside phosphorylase, is a key regulator of purine metabolism and may influence UCP1 activity (54). *Far1* encodes fatty acly-CoA reductase, a peroxisome enzyme essential for the synthesis of ether phospholipids, including plasmalogens (55). Collectively, these findings suggest that epigenetic perturbations induced by the Ebf2 variant contribute to widespread dysregulation across pathways governing fatty acid metabolism, ECM remodeling, and inflammatory cytokine signaling (56).

Effects of *EBF2* and *EBF2* (1-164) on human adipocyte differentiation and gene expression

The dominant-negative effect exerted by the truncated *EBF2* nonsense variant was reproduced in human preadipocytes. Expression of the *EBF2* variant in human preadipocytes decreased adipogenesis, as shown by reduced lipid droplet staining (Figure 7, A and B). We performed unbiased bulk RNA sequencing of human preadipocytes transduced with lentivirus constructs of control, full-length EBF2, and truncated EBF2 (1-164) and induced to differentiate into adipocytes (Figure 7C, GSE288824). *EBF2* and *EBF2* (1-164) led to differential gene expression of PI3K-AKT, ECM, and cytokine-cytokine receptor interaction pathways (Figure 7, D and E), mirroring the changes observed in the IWAT of *Ebf2*$^{E165X/+}$ mice. Cells transduced with *EBF2* (1-164) variant demonstrated reduced expression of *COL1A1*, *COL1A2*, *COL4A1*, *THBS1*, and *TNXB*, along with increased expression of *LAMB3*, *SPP1*, *LAMA1*, *ITGA10*, and *ITGA5* (Figure 7D). Additionally, *EBF2* (1-164) increased the expression of specific cytokines and growth factors, including *IL1A*, *IL1B*, *CXCL2*, *CCL5*, *IL24*, and *TGFB2* (Figure 7E). These findings suggest that the nonsense *EBF2* variant disrupts gene expression in key biological pathways, including the PI3K-AKT-mTOR signaling pathway, ECM remodeling, and cytokine-cytokine receptor interactions, in both mice and humans.

Fibrotic and inflamed adipose tissue in the patient with *EBF2* p.E165X variant

Given increased numbers of CD34^{+} cells, coupled with excess ECM deposition in Ebf2E165X/+ mice and altered ECM and cytokine expression in human adipocytes, we sought to determine adipose tissue ECM composition and immunophenotype in our patient using imaging cytometry by time-of-flight (CyTOF). Imaging by CyTOF identified infiltration of neutrophils (CD15+ cells), monocytes/macrophages (CD11c+ and CD68+ cells), and CD34+ cells in the patient's WAT, highlighting the complexity of the stromal cell population in this tissue (Figure 7F). Furthermore, CyTOF imaging revealed significant type I collagen deposition, surrounded by CD34+ cells and elevated levels of macrophages ($CD68^+$ cells) (Figure 7G). These findings were corroborated by immunofluorescent staining, which showed reduced PLIN1+ adipocytes, increased type I collagen deposition, and increased prevalence of CD34+ cells (Figures 7H and 7I). The accumulation of ECM proteins, an increased number of $CD34^+$ stromal cells, and the infiltration of myeloid and lymphoid cells are histological features shared between the *Ebf2* variant mouse model and the patient, underscoring their pathological similarity.

Discussion

In this study, we identified an *EBF2* p.E165X variant in a patient with atypical PLD, thereby uncovering the critical role of EBF2 in regulating adipogenesis and ECM remodeling. To our knowledge, this is the first report linking *EBF2* dysfunction to PLD syndromes. Advances in genetic technology have identified an expanding number of candidate gene variants that may underlie PLD. However, functional characterization and validation of newly identified gene variants remain challenging, highlighting a translational research gap between clinical and genetic studies of lipodystrophy syndromes and the broader field of adipose tissue biology, as is the case with other rare diseases. Our study provides critical evidence linking the *EBF2* p.E165X variant to impaired adipogenesis and adipose tissue function, thereby bridging a crucial gap between genotype and phenotype in understanding the pathogenesis of lipodystrophy in this patient.

The *Ebf* family, including *Ebf1* and *Ebf2*, regulates mouse adipogenesis in vitro (8, 57, 58) and plays a key role in adipocyte differentiation and the development of white and brown adipose tissues (15, 16, 59, 60). However, the role of the *EBF* family in human adipose tissue development remains undefined. To gather more convincing evidence and address the limitations of in vitro assays, we developed *Ebf2* p.E165X heterozygous KI ($Ebf2^{E165X/+}$) mice. These mice were fertile and exhibited no discernible defects at birth. However, we obtained a very few homozygous KI ($Ebf2^{E165X/E165X}$) mice on a mixed genetic background and none on a C57BL/6 background, suggesting that either a complete loss of *Ebf2* or an increased gene dosage of the *Ebf2* p.E165X variant may have caused a lethal phenotype. The $Ebf2^{E165X/E165X}$ mouse showed restricted WAT development with excess ECM deposition. The lethality of the $Ebf2^{E165X/E165X}$ mice contrasts sharply with the phenotype of the whole-body *Ebf2*-null mice, which are not lethal but display a wide array of biological impairments in the migration of gonadotropin-releasing hormone (GnRH) neurons (61), peripheral nerve myelination (62, 63), bone development (13), brown adipose tissue development (16), and white adipose tissue beiging (64). These biological phenotypes may explain some of the clinical features of our patient (delayed puberty, scoliosis, hand contracture, pain hypersensitivity). However, unlike global *Ebf2* knockout mice, *Ebf2*$^{E165X/E165X}$ mice showed near-complete neonatal lethality, suggesting that the *EBF2* (1-164) variant exerts a more severe impact on peri- and postnatal development than would be expected from its loss of function. Our study demonstrates that the *Ebf2* variant broadly disrupts H3K27Ac recruitment to multiple transcription factor motifs in adipose stromal cells, highlighting the detrimental impact of the truncated protein on transcriptional networks, which may have contributed to the near-lethal phenotype of *Ebf2*$^{E165X/E165X}$ mice.

Adipose tissue fibrosis or excess ECM deposition is observed in obesity and lipodystrophy (65, 66). Tissue fibrosis is often viewed as a consequence of inflammation; however, the precise sequence and interplay between inflammation and fibrosis in the development of diabetes remain poorly understood (67). At 4 weeks of age, the adipose tissue structure in *Ebf2*$^{E165X/+}$ mice appeared identical to that of *Ebf2*$^{+/+}$ mice, before the onset of adult WAT expansion. Before post-weaning WAT expansion, adipose tissue was densely packed with numerous small adipocytes, each encased in collagen fibers (22, 46). Between 4 and 16 weeks of age, *Ebf2*$^{+/+}$ IWAT displayed uniform hypertrophy of adipocytes with the diminution of collagens and fibronectin content and the decreasing number of CD34^{+} cells. In contrast, *Ebf2*$^{\mathrm{E165X/+}}$ mice showed dysmorphic adipocyte hypertrophy, with persistent collagen and fibronectin deposition, indicating restricted adipogenesis and impaired ECM remodeling, resulting in IWAT fibrosis (22, 48). These findings suggest that excess ECM deposition in adipose tissues of *Ebf2*$^{\mathrm{E165X/+}}$ mice occurs during the post-weaning stages of WAT expansion, when adipogenesis and ECM remodeling need to be coordinated.

Mitochondrial biogenesis and function are crucial for the healthy development and expansion of adipose tissue (68). As mentioned earlier, at 4 weeks of age, *Ebf2*$^{\mathrm{E165X/+}}$ IWAT did not exhibit noticeable differences from *Ebf2*$^{+/+}$ IWAT, as observed through H&E and immunofluorescent staining of CD34^{+} cells and ECM proteins. However, bulk RNA-sequencing of IWAT revealed mitochondrial gene suppression and reduced expression of *Ucp1*, *Cidea*, and *Ppara*. These genes are expressed in mitochondria-rich brown and beige adipocytes, suggesting that the *Ebf2* nonsense variant may interfere with mitochondrial function (16, 42, 64). This indicates that early perinatal adipose tissue development may not require extensive mitochondrial involvement. During the pre-weaning phase, mice primarily rely on free fatty acids as an energy source rather than carbohydrates for growth, and adipocytes can directly absorb free fatty acids (69). Following weaning, white adipose tissue expands with *de novo* lipogenesis as mice are transitioned to a carbohydrate-rich diet, with the induction of enzymes involved in fatty acid synthesis, such as acetyl CoA carboxylase (*Acc*) and ATP citrate lyase (*Acly*) (70). Notably, 4-week-old *Ebf2*$^{\mathrm{E165X/+}}$ IWAT showed comparable levels of *Fatp1* (*Slc27A1*), *Cd36*, *Ascl1*, *Fabp4*, and *Lipe*, which are involved in free fatty acid uptake and retention. Moreover, the expression of *Insr* and *Igf1r,* key regulators of adipose tissue expansion (71), was comparable between 4-week-old *Ebf2*$^{E165X/+}$ and *Ebf2*$^{+/+}$ mice. However, maladaptation to a carbohydrate-rich diet might have occurred in *Ebf2*$^{E165X/+}$ mice due to the suppressed expression of mitochondrial genes, including *Aco2* (72), *Hadha*, and *Hadhb* (73). Decreased oxidative phosphorylation, driven by downregulated mitochondrial genes, may have led to ineffective de novo lipogenesis and impaired adipocyte maturation (74). Despite these changes, bulk RNA-seq data showed abundant expression of mitochondrially encoded genes, including *Mt-Atp8*, *Mt-Co1*, *Mt-Cytb*, and *Mt-Nd1* in *Ebf2*$^{E165X/+}$ IWAT. TEM examination of IWAT did not reveal a significant decrease in mitochondrial number, despite their morphological abnormalities and association with lipid droplets. These findings suggest that adipose tissue mitochondrial dysfunction in postnatal IWAT in *Ebf2*$^{E165X/+}$ mice is likely caused by the selective downregulation of nuclear-encoded mitochondrial genes due to EBF2 dysfunction.

Adipose tissue plasticity, homeostasis, and metabolic consequences can be assessed in vivo through HFD challenges (67). *Ebf2*$^{E165X/+}$ mice with 45% HFD demonstrated hypertrophic adipocytes of variable sizes, excess ECM deposition, tissue macrophage infiltration, liver steatosis, and glucose intolerance compared with *Ebf2*$^{+/+}$ mice. These adipose tissue and metabolic phenotypes resemble clinical presentations of patients with PLD (2, 35, 75). Moreover, serum leptin and adiponectin levels became significantly lower in *Ebf2*$^{E165X/+}$ mice than in *Ebf2*$^{+/+}$ mice after the HFD challenge, suggesting that the diet is a critical modifier of genetically predisposed adipose tissues. These findings align with the diagnostic challenges of PLD, as these patients often present to clinics only after developing prediabetes, metabolic-associated steatohepatitis (MASH), dyslipidemia, and kidney disease as adults. Notably, when these mice were maintained on a chow diet, they did not show metabolic deterioration at 16 weeks of age despite the disrupted adipose tissue structure. This suggests that dietary modification potentially mitigates adipose dysfunction and metabolic decline in PLD caused by EBF2 dysfunction.

Mouse models may not fully capture the heterogeneity of human adipose tissue depots and their functions, particularly subcutaneous adipose tissue (13, 61, 64). However, *Ebf2*$^{\mathrm{E165X/+}}$ mice showed restricted adipose tissue expansion characterized by dysmorphic adipocyte hypertrophy and excess ECM deposition, particularly in the IWAT of males and females, increased macrophage infiltration, and glucose intolerance in male mice. Our study included a sufficient number of female mice and confirmed restricted adipogenesis, excess ECM deposition, and decreased leptin and adiponectin levels in *Ebf2*$^{E165X/+}$ female mice. However, C57BL/6J female mice are resistant to HFD-induced obesity and diabetes, most likely due to increased energy expenditure compared to male mice and the protective effect of estrogen (76). Prolonged HFD and ovariectomy or estrogen receptor blockade may further improve the utility of *Ebf2*$^{E165X/+}$ female mice for disease modeling for women with PLD syndromes (2). Detailed examination of sexual dimorphism, the effects of aging, and various dietary interventions may further refine the utility of *Ebf2*$^{E165X/+}$ mice as a PLD animal model (77).

Our findings align with the biological role of *EBF2* in humans, as suggested by several lines of existing evidence. *EBF2* marks a subset of human adipocytes that correlates with increased BMI (18). An *EBF2* common variant was associated with visceral adipose tissue mass assessed with MRI (20). Our investigation of published and publicly available databases suggests close associations between EBF2 common variants and metabolic traits (diabetes, hypertension, and hypertriglyceridemia), overlapping with those of metabolic syndrome (31-33, 75). Lipodystrophy-like abnormal fat distribution and gene polymorphisms associated with lipodystrophy syndromes were observed in subclusters of individuals with diabetes (34) and cardiovascular diseases (35, 78). Consistent with these SNP association studies, lipodystrophy-associated metabolic deterioration observed in our patient with the pathogenic *EBF2* variant supports a critical role for EBF2 in maintaining metabolic homeostasis. Another *EBF* family member, *EBF1* is expressed higher in functional, hyperplastic adipocytes relative to hypertrophic adipocytes in humans, and EBF-like binding motif was enriched in adipogenic genes, such as *PPARG*, *NCOR2*, *LIPE*, *PNPLA2*, *PLIN1*, and *CIDEC* (15).

Our in vitro studies indicate that the *Ebf2* p.E165X variant impairs adipocyte lipid accumulation in a cell-autonomous and dominant-negative manner despite the presence of other *Ebf* family members, including *Ebf1* and *Ebf3*. In contrast, reporter assays using a synthetic EBF-consensus element in a heterologous cell line did not reveal a dominant-negative effect of the truncated EBF2 protein on EBF1- or EBF3-dependent transcriptional activation. These findings suggest that the pathogenic effects of the *EBF2* variant are unlikely to reflect direct inhibition of EBF family DNA-binding activity, but instead arise from context-dependent disruption of the broader transcriptional regulatory programs that govern adipocyte differentiation, including ZNF423 and ZNF521. The broader impact of the *EBF2* variant was indeed supported by the significantly altered chromatin accessibility, as assessed by H3K27Ac enhancer binding.

Dominant negative variants of transcription factors contribute to the pathogenesis of a broad spectrum of diseases (79), including familial PLD, type 3 (FPLD3) caused by PPARG variants (80), combined pituitary hormone deficiency (CPHD) associated with POU1F1 (PIT1) variants (81), and generalized thyroid hormone resistance (GRTH) due to THRB variants (82). Emerging therapeutic strategies include the targeted degradation of pathogenic variant proteins using proteolysis-targeting chimeras (PROTAC) (83), suppression or splicing modulation of variant mRNAs with antisense oligonucleotides (ASOs) (84), and ex vivo gene editing followed by the transplantation of patient-derived adipose stem cells (85). These therapeutic modalities need to be explored and tested for the prevention and treatment of lipodystrophy syndromes caused by harmful variant proteins.

Despite genetic causality of lipodystrophy being supported by in vivo and in vitro modeling, our study is limited by reliance on a single family. However, the strength of existing genetic evidence from large databases and the previous linkage of the gene to adipogenesis are all supportive and reproducible findings. Moreover, our mouse model is a whole-body KI; therefore, the *EBF2* p.E165X variant may have exerted additional biological effects in cell types other than adipocytes. Nonetheless, our in vitro study with primary SVF showed that the *EBF2* p.E165X variant has a deleterious impact on adipocyte differentiation in a cell-autonomous manner, with variant transcript levels comparable to wild-type *Ebf2* in our KI mouse model. However, due to the unavailability of the antibody that detects the N-terminal portion of EBF2/Ebf2, we were not able to demonstrate the presence of the truncated EBF2 variant protein in this study. While it is interesting that our patient exhibited additional phenotypic features that may be linked to EBF2 function, such as hypogonadotropic hypogonadism, bone and skeletal developmental abnormalities (including hand contracture and scoliosis), umbilical hernia, and Alport-like kidney pathology, we have not examined these organ systems in detail in the knock-in mouse model.

In conclusion, our in vitro and in vivo investigations indicate that EBF2 dysfunction caused by the *EBF2* p.E165X variant compromises adipose tissue expansion and remodeling, ultimately leading to metabolic dysregulation. The discovery of a pathogenic *EBF2* variant in our patient helped us unravel the indispensable role of EBF2 in healthy adipose tissue expansion and function.

Methods

Sex as a biological variable

Our study examined male and female animals, and similar findings are reported for both sexes. We considered sex a modifier wherever possible. When our study examined the interaction between genotypes and diet, the effect was analyzed in females and males respectively.

Human subjects

The proband has been followed at the University of Michigan since age 11, participating in the LDLync natural history study (NCT03087253) and prior phenotyping/biopsy studies (NCT01679197, NCT00596934). Clinical data were extracted from medical records and the LDLync registry. DNA analyses were conducted through our tissue and blood biorepository (IRBMED: HUM00062732). Healthy adipose tissue was obtained from a 33-year-old female donor (IRBMED: HUM00174659).

Mouse model

Ebf2$^{E165/X}$ knock-in mice were generated on a C57BL/6J background (#000664, Jackson Laboratory) using CRISPR/Cas9 at the University of Michigan Transgenic Core.

Cell culture

3T3-L1, HEK293, and human subcutaneous preadipocytes were cultured in DMEM with 10% FBS. Adipogenesis was induced in 3T3-L1 cells with dexamethasone, insulin, and IBMX, or in human preadipocytes and SVFs with insulin, rosiglitazone, and T3.

Human genetic sequencing

Exome sequencing (Roche NimbleGen v3.0, HiSeq2000, ~50×) and genome sequencing (PCR-free HiSeq X Ten, ~30×) were performed at Michigan and the Broad Institute, respectively. Reads were aligned to hg38 with BWA, processed with Picard/GATK, and variants called with HaplotypeCaller, filtered with VQSR, and annotated with VEP. Structural variants were detected with GATK-SV, mtDNA variants with gnomAD-mitochondria and MitoSAlt, and tandem repeat expansions with ExpansionHunter v5.

Molecular assays

Standard protocols were used for SVF isolation, RNAi and lentiviral transduction, luciferase reporter assays, RT-qPCR, immunofluorescence, lipid droplet staining, histology, TEM, RNA-seq, and CUT&RUN (anti-H3K27Ac; analysis with Bowtie2, MACS2, and HOMER). Details, oligonucleotide sequences, and antibody information are provided in Supplemental Methods and Tables.

Statistics

Experiments included ≥3 biological replicates. Data are mean ± SEM. Comparisons were performed using Student's t-test or two-way ANOVA with post-hoc Tukey testing (GraphPad Prism 10). Sex was included as a modifier in animal studies. $p < 0.05$ was considered significant.

Study approval

All human protocols were IRB-approved with written informed consent. The University of Michigan IACUC approved animal studies.

Data availability

RNA-seq data are available at GEO (GSE288829, GSE288824). All other data are provided in the main text or Supplemental Data. All values presented in the figures are provided in the Supporting Data Values file.

Authors' contributions

MF-F and DG are co-first authors. MF-F conducted experiments, analyzed and collected patient data, organized figures for the initial submission, and drafted the manuscript. DG performed experiments, collected and analyzed animal data, organized figures for the revision, and co-wrote the manuscript. The first authorship order was determined by mutual agreement of the authors. LP analyzed genome sequencing data and reviewed drafts. RKV and EDB performed animal experiments and data collection. MO'L, HLR, CG, KR, and MSU provided variant interpretation and manuscript review. AMR contributed to experiments and to discussions of results. AN collected patient data. PS provided experimental guidance, participated in result discussions, and edited the manuscript. EAO conceived the project, assembled the team, coordinated collaborations, supervised patient studies, provided clinical care, secured funding, reviewed analyses, and co-wrote the manuscript. THC designed and supervised laboratory experiments, curated data, performed final analyses, and co-wrote the manuscript. All authors critically reviewed and approved the manuscript. EAO and THC share responsibility for data integrity.

Acknowledgments

We thank our patient and her mother for inspiring this research. This work is the result of NIH funding, in whole or in part, and is subject to the NIH Public Access Policy. Under this federal funding, the NIH has been authorized to make the work publicly available in PubMed Central. Clinical phenotyping was supported by NIH grant R01-DK088114 (Oral, Conjeevaram) and the Lipodystrophy Research Fund at the University of Michigan (Sopha Family, Baker Family, Rosenblum Family, White Point Foundation of Turkey). RNA-seq was partially supported by R01-DK125513 (Oral, MacDougald). Infrastructure support was provided by NIH grants 2P30DK089503, 5P30DK020572, UL1TR002240, and the Caswell Diabetes Institute. Whole genome sequencing was provided by the Broad CMG, supported by NIH grant K23DK114551, NHGRI grants UM1HG008900 and R01HG009141 (with additional support from NEI and NHLBI), and a Chan Zuckerberg Initiative grant (DAF2019-199278). We thank the University of Michigan Vector Core (Thomas Lanigan, Roland Hilgart) for designing and preparing the vector and lentivirus constructs, the Transgenic Animal Model Core (Thomas L. Saunders, Zachary T. Freeman, Elizabeth Hughes, Wanda Filipiak, Galina Gabrilina, Honglai Zhang) for generating *Ebf2*$^{E165/X}$ mice, the CyTOF Core (Fei Wen, Syed Rizvi) for imaging cytometry, and the Flow Cytometry Core (David Adams). We also thank the University of Pisa for supporting DG's lipodystrophy research.

References

1. Brown RJ, Araujo-Vilar D, Cheung PT, Dunger D, Garg A, Jack M, et al. The Diagnosis and Management of Lipodystrophy Syndromes: A Multi-Society Practice Guideline. *J Clin Endocrinol Metab.* 2016;101(12):4500-11.
2. Foss-Freitas MC, Akinci B, Luo Y, Stratton A, and Oral EA. Diagnostic strategies and clinical management of lipodystrophy. *Expert Rev Endocrinol Metab.* 2020;15(2):95-114.
3. Garg A. Acquired and Inherited Lipodystrophies. *N. Engl. J. Med..* 2004;350(12):1220-34.
4. Mosbah H, Akinci B, Araújo-Vilar D, Carrion Tudela J, Ceccarini G, Collas P, et al. Proceedings of the annual meeting of the European Consortium of Lipodystrophies (ECLip) Cambridge, UK, 7-8 April 2022. *Ann Endocrinol (Paris).* 2022;83(6):461-8.
5. Akinci B, Meral R, Rus D, Hench R, Neidert AH, DiPaola F, et al. The complicated clinical course in a case of atypical lipodystrophy after development of neutralizing antibody to metreleptin: treatment with setmelanotide. *Endocrinol Diabetes Metab Case Rep.* 2020;2020.
6. Altarejos JY, Pangilinan J, Podgrabinska S, Akinci B, Foss-Freitas M, Neidert AH, et al. Preclinical, randomized phase 1, and compassionate use evaluation of REGN4461, a leptin receptor agonist antibody for leptin deficiency. *Sci Transl Med.* 2023;15(723):eadd4897.
7. Liao D. Emerging Roles of the EBF Family of Transcription Factors in Tumor Suppression. *Mol. Cancer Res..* 2009;7(12):1893-901.
8. Jimenez MA, Akerblad P, Sigvardsson M, and Rosen ED. Critical role for Ebf1 and Ebf2 in the adipogenic transcriptional cascade. *Mol Cell Biol.* 2007;27(2):743-57.
9. Kieslinger M, Hiechinger S, Dobreva G, Consalez GG, and Grosschedl R. Early B cell factor 2 regulates hematopoietic stem cell homeostasis in a cell-nonautonomous

manner. *Cell Stem Cell.* 2010;7(4):496-507.

10. Dubois L, and Vincent A. The COE--Collier/Olf1/EBF--transcription factors: structural conservation and diversity of developmental functions. *Mech Dev.* 2001;108(1-2):3-12.

11. Tsai RY, and Reed RR. Cloning and functional characterization of Roaz, a zinc finger protein that interacts with O/E-1 to regulate gene expression: implications for olfactory neuronal development. *J Neurosci.* 1997;17(11):4159-69.

12. Hata A, Seoane J, Lagna G, Montalvo E, Hemmati-Brivanlou A, and Massagué J. OAZ uses distinct DNA- and protein-binding zinc fingers in separate BMP-Smad and Olf signaling pathways. *Cell.* 2000;100(2):229-40.

13. Kieslinger M, Folberth S, Dobreva G, Dorn T, Croci L, Erben R, et al. EBF2 regulates osteoblast-dependent differentiation of osteoclasts. *Dev Cell.* 2005;9(6):757-67.

14. Green YS, and Vetter ML. EBF proteins participate in transcriptional regulation of Xenopus muscle development. *Dev Biol.* 2011;358(1):240-50.

15. Gao H, Mejhert N, Jackie, Arner E, Lorente-Cebrián S, Ehrlund A, et al. Early B Cell Factor 1 Regulates Adipocyte Morphology and Lipolysis in White Adipose Tissue. *Cell Metab.* 2014;19(6):981-92.

16. Rajakumari S, Wu J, Ishibashi J, Lim H-W, Giang A-H, Won K-J, et al. EBF2 Determines and Maintains Brown Adipocyte Identity. *Cell Metab.* 2013;17(4):562-74.

17. Shao M, Ishibashi J, Kusminski CM, Wang QA, Hepler C, Vishvanath L, et al. Zfp423 Maintains White Adipocyte Identity through Suppression of the Beige Cell Thermogenic Gene Program. *Cell Metab.* 2016;23(6):1167-84.

18. Emont MP, Jacobs C, Essene AL, Pant D, Tenen D, Colleluori G, et al. A single-cell atlas of human and mouse white adipose tissue. *Nature.* 2022;603(7903):926-33.

19. Wain LV, Vaez A, Jansen R, Joehanes R, van der Most PJ, Erzurumluoglu AM, et al. Novel Blood Pressure Locus and Gene Discovery Using Genome-Wide Association Study and Expression Data Sets From Blood and the Kidney. *Hypertension.*

2017;70(3):e4-e19.

20. Agrawal S, Wang M, Klarqvist MDR, Smith K, Shin J, Dashti H, et al. Inherited basis of visceral, abdominal subcutaneous and gluteofemoral fat depots. *Nature Communications.* 2022;13(1).

21. Hofwimmer K, de Paula Souza J, Subramanian N, Vujičić M, Rachid L, Méreau H, et al. IL-1β promotes adipogenesis by directly targeting adipocyte precursors. *Nature Commun.* 2024;15(1):7957.

22. Chun TH, Hotary KB, Sabeh F, Saltiel AR, Allen ED, and Weiss SJ. A pericellular collagenase directs the 3-dimensional development of white adipose tissue. *Cell.* 2006;125(3):577-91.

23. Hikage F, Atkins S, Kahana A, Smith TJ, and Chun TH. HIF2A-LOX Pathway Promotes Fibrotic Tissue Remodeling in Thyroid-Associated Orbitopathy. *Endocrinology.* 2019;160(1):20-35.

24. Trayhurn P. Hypoxia and Adipose Tissue Function and Dysfunction in Obesity. *Physiol. Rev.* 2013;93(1):1-21.

25. Satoor SN, Puranik AS, Kumar S, Williams MD, Ghale M, Rahalkar A, et al. Location, location, location: Beneficial effects of autologous fat transplantation. *Sci. Rep.*2011;1(1).

26. Macotela Y, Emanuelli B, Mori MA, Gesta S, Schulz TJ, Tseng Y-H, et al. Intrinsic Differences in Adipocyte Precursor Cells From Different White Fat Depots. *Diabetes.* 2012;61(7):1691-9.

27. Jeffery E, Wing A, Holtrup B, Sebo Z, Jennifer, Saavedra-Peña R, et al. The Adipose Tissue Microenvironment Regulates Depot-Specific Adipogenesis in Obesity. *Cell Metab.* 2016;24(1):142-50.

28. Tang W, Zeve D, Suh JM, Bosnakovski D, Kyba M, Hammer RE, et al. White Fat Progenitor Cells Reside in the Adipose Vasculature. *Science.* 2008;322(5901):583-6.

29. Wang QA, Tao C, Gupta RK, and Scherer PE. Tracking adipogenesis during white

adipose tissue development, expansion and regeneration. *Nat Med.* 2013;19(10):1338-44.

30. Jeffery E, Church CD, Holtrup B, Colman L, and Rodeheffer MS. Rapid depot-specific activation of adipocyte precursor cells at the onset of obesity. *Nat Cell Biol.* 2015;17(4):376-85.
31. Suzuki K, Hatzikotoulas K, Southam L, Taylor HJ, Yin X, Lorenz KM, et al. Genetic drivers of heterogeneity in type 2 diabetes pathophysiology. *Nature.* 2024;627(8003):347-57.
32. Graham SE, Clarke SL, Wu KH, Kanoni S, Zajac GJM, Ramdas S, et al. The power of genetic diversity in genome-wide association studies of lipids. *Nature.* 2021;600(7890):675-9.
33. Zhu Z, Wang X, Li X, Lin Y, Shen S, Liu CL, et al. Genetic overlap of chronic obstructive pulmonary disease and cardiovascular disease-related traits: a large-scale genome-wide cross-trait analysis. *Respir Res.* 2019;20(1):64.
34. Udler MS, Kim J, von Grotthuss M, Bonàs-Guarch S, Cole JB, Chiou J, et al. Type 2 diabetes genetic loci informed by multi-trait associations point to disease mechanisms and subtypes: A soft clustering analysis. *PLoS Med.* 2018;15(9):e1002654.
35. Akinci B, von Schnurbein J, Araujo-Vilar D, Wabitsch M, and Oral EA. Lipodystrophy Prevalence, “Lipodystrophy-Like Phenotypes,” and Diagnostic Challenges. *Diabetes.* 2024;73(7):1039-42.
36. Jurgens SJ, Choi SH, Morrill VN, Chaffin M, Pirruccello JP, Halford JL, et al. Analysis of rare genetic variation underlying cardiometabolic diseases and traits among 200,000 individuals in the UK Biobank. *Nat Genet.* 2022;54(3):240-50.
37. Singer-Berk M, Gudmundsson S, Baxter S, Seaby EG, England E, Wood JC, et al. Advanced variant classification framework reduces the false positive rate of predicted loss-of-function variants in population sequencing data. *Am. J. Hum. Genet.*

2023;110(9):1496-508.

38. Samocha KE, Robinson EB, Sanders SJ, Stevens C, Sabo A, McGrath LM, et al. A framework for the interpretation of de novo mutation in human disease. *Nat Genet.* 2014;46(9):944-50.
39. Codner GF, Mianné J, Caulder A, Loeffler J, Fell R, King R, et al. Application of long single-stranded DNA donors in genome editing: generation and validation of mouse mutants. *BMC Biol.* 2018;16(1):70.
40. Gupta RK, Arany Z, Seale P, Mepani RJ, Ye L, Conroe HM, et al. Transcriptional control of preadipocyte determination by Zfp423. *Nature.* 2010;464(7288):619-23.
41. Addison WN, Fu MM, Yang HX, Lin Z, Nagano K, Gori F, et al. Direct transcriptional repression of Zfp423 by Zfp521 mediates a bone morphogenic protein-dependent osteoblast versus adipocyte lineage commitment switch. *Mol Cell Biol.* 2014;34(16):3076-85.
42. Shao M, Zhang Q, Truong A, Shan B, Vishvanath L, Li L, et al. ZFP423 controls EBF2 coactivator recruitment and PPARγ occupancy to determine the thermogenic plasticity of adipocytes. *Gene Dev.* 2021.
43. Mega T, Lupia M, Amodio N, Horton SJ, Mesuraca M, Pelaggi D, et al. Zinc finger protein 521 antagonizes early B-cell factor 1 and modulates the B-lymphoid differentiation of primary hematopoietic progenitors. *Cell Cycle.* 2011;10(13):2129-39.
44. Travis A, Hagman J, Hwang L, and Grosschedl R. Purification of early-B-cell factor and characterization of its DNA-binding specificity. *Mol. Cell. Biol.* 1993;13(6):3392-400.
45. Scicchitano S, Giordano M, Lucchino V, Montalcini Y, Chiarella E, Aloisio A, et al. The stem cell-associated transcription co-factor, ZNF521, interacts with GLI1 and GLI2 and enhances the activity of the Sonic hedgehog pathway. *Cell Death Dis.* 2019;10(10):715.
46. Napolitano L. THE DIFFERENTIATION OF WHITE ADIPOSE CELLS. AN ELECTRON

MICROSCOPE STUDY. *J Cell Biol.* 1963;18(3):663-79.

47. Khan T, Muise ES, Iyengar P, Wang ZV, Chandalia M, Abate N, et al. Metabolic dysregulation and adipose tissue fibrosis: role of collagen VI. *Mol Cell Biol.* 2009;29(6):1575-91.

48. Sun K, Tordjman J, Clément K, and Scherer Philipp E. Fibrosis and Adipose Tissue Dysfunction. *Cell Metab.* 2013;18(4):470-7.

49. Hinte LC, Castellano-Castillo D, Ghosh A, Melrose K, Gasser E, Noé F, et al. Adipose tissue retains an epigenetic memory of obesity after weight loss. *Nature.* 2024;636(8042):457-65.

50. Marcelin G, Ferreira A, Liu Y, Atlan M, Aron-Wisnewsky J, Pelloux V, et al. A PDGFRα-Mediated Switch toward CD9(high) Adipocyte Progenitors Controls Obesity-Induced Adipose Tissue Fibrosis. *Cell Metab.* 2017;25(3):673-85.

51. Iwayama T, Steele C, Yao L, Dozmorov MG, Karamichos D, Wren JD, et al. PDGFRα signaling drives adipose tissue fibrosis by targeting progenitor cell plasticity. *Genes Dev.* 2015;29(11):1106-19.

52. Guo L, Huang JX, Liu Y, Li X, Zhou SR, Qian SW, et al. Transactivation of Atg4b by C/EBPβ promotes autophagy to facilitate adipogenesis. *Mol Cell Biol.* 2013;33(16):3180-90.

53. Lahnalampi M, Heinäniemi M, Sinkkonen L, Wabitsch M, and Carlberg C. Time-Resolved Expression Profiling of the Nuclear Receptor Superfamily in Human Adipogenesis. *PLOS ONE.* 2010;5(9):e12991.

54. Fromme T, Kleigrewe K, Dunkel A, Retzler A, Li Y, Maurer S, et al. Degradation of brown adipocyte purine nucleotides regulates uncoupling protein 1 activity. *Mol Metab.* 2018;8:77-85.

55. Honsho M, Asaoku S, and Fujiki Y. Posttranslational Regulation of Fatty Acyl-CoA Reductase 1, Far1, Controls Ether Glycerophospholipid Synthesis*♦. *J Biol Chem.*

2010;285(12):8537-42.

56. Roh HC, Kumari M, Taleb S, Tenen D, Jacobs C, Lyubetskaya A, et al. Adipocytes fail to maintain cellular identity during obesity due to reduced PPARgamma activity and elevated TGFbeta-SMAD signaling. *Mol Metab.* 2020;42:101086.

57. Akerblad P, Lind U, Liberg D, Bamberg K, and Sigvardsson M. Early B-cell factor (O/E-1) is a promoter of adipogenesis and involved in control of genes important for terminal adipocyte differentiation. *Mol Cell Biol.* 2002;22(22):8015-25.

58. Åkerblad P, Månsson R, Lagergren A, Westerlund S, Basta B, Lind U, et al. Gene expression analysis suggests that EBF-1 and PPARγ2 induce adipogenesis of NIH-3T3 cells with similar efficiency and kinetics. *Physiol. Genomics.* 2005;23(2):206-16.

59. Fretz JA, Nelson T, Xi Y, Adams DJ, Rosen CJ, and Horowitz MC. Altered metabolism and lipodystrophy in the early B-cell factor 1-deficient mouse. *Endocrinology.* 2010;151(4):1611-21.

60. Griffin MJ, Zhou Y, Kang S, Zhang X, Mikkelsen TS, and Rosen ED. Early B-cell factor-1 (EBF1) is a key regulator of metabolic and inflammatory signaling pathways in mature adipocytes. *J Biol Chem.* 2013;288(50):35925-39.

61. Corradi A, Croci L, Broccoli V, Zecchini S, Previtali S, Wurst W, et al. Hypogonadotropic hypogonadism and peripheral neuropathy in Ebf2-null mice. *Development.* 2003;130(2):401-10.

62. Giacomini C, La Padula V, Schenone A, Leandri M, Contestabile A, Moruzzo D, et al. Both Schwann cell and axonal defects cause motor peripheral neuropathy in Ebf2-/- mice. *Neurobiol Dis.* 2011;42(1):73-84.

63. Moruzzo D, Nobbio L, Sterlini B, Consalez GG, Benfenati F, Schenone A, et al. The Transcription Factors EBF1 and EBF2 Are Positive Regulators of Myelination in Schwann Cells. *Mol Neurobiol.* 2017;54(10):8117-27.

64. Stine RR, Shapira SN, Lim HW, Ishibashi J, Harms M, Won KJ, et al. EBF2 promotes

the recruitment of beige adipocytes in white adipose tissue. *Mol Metab.* 2016;5(1):57-65.

65. Gandotra S, Dour CL, Bottomley W, Cervera P, Giral P, Reznik Y, et al. Perilipin Deficiency and Autosomal Dominant Partial Lipodystrophy. *N. Engl. J. Med.* 2011;364(8):740-8.

66. Divoux A, Tordjman J, Lacasa D, Veyrie N, Hugol D, Aissat A, et al. Fibrosis in human adipose tissue: composition, distribution, and link with lipid metabolism and fat mass loss. *Diabetes.* 2010;59(11):2817-25.

67. Klein S, Gastaldelli A, Yki-Järvinen H, and Scherer PE. Why does obesity cause diabetes? *Cell Metab.* 2022;34(1):11-20.

68. Kusminski CM, and Scherer PE. Mitochondrial dysfunction in white adipose tissue. *Trends Endocrinol Metab.* 2012;23(9):435-43.

69. D'Agostino D, Cordle RA, Kullman J, Erlanson-Albertsson C, Muglia LJ, and Lowe ME. Decreased Postnatal Survival and Altered Body Weight Regulation in Procolipase-deficient Mice *. *J Biol Chem.* 2002;277(9):7170-7.

70. Tsujikawa M, and Kimura S. Changes in lipid synthesis in rat adipose tissue during development. *J Nutr Sci Vitaminol (Tokyo).* 1980;26(4):367-74.

71. Boucher J, Softic S, El Ouaamari A, Krumpoch MT, Kleinridders A, Kulkarni RN, et al. Differential Roles of Insulin and IGF-1 Receptors in Adipose Tissue Development and Function. *Diabetes.* 2016;65(8):2201-13.

72. Chen Y, Cai GH, Xia B, Wang X, Zhang CC, Xie BC, et al. Mitochondrial aconitase controls adipogenesis through mediation of cellular ATP production. *Faseb J.* 2020;34(5):6688-702.

73. Aldehoff AS, Karkossa I, Goerdeler C, Krieg L, Schor J, Engelmann B, et al. Unveiling the dynamics of acetylation and phosphorylation in SGBS and 3T3-L1 adipogenesis. *iScience.* 2024;27(6).

74. Vernochet C, Damilano F, Mourier A, Bezy O, Mori MA, Smyth G, et al. Adipose tissue

mitochondrial dysfunction triggers a lipodystrophic syndrome with insulin resistance, hepatosteatosis, and cardiovascular complications. *Faseb J.* 2014;28(10):4408-19.

75. Mann JP, and Savage DB. What lipodystrophies teach us about the metabolic syndrome. *J. Clin. Invest.* 2019;129(10):4009-21.

76. Handgraaf S, Riant E, Fabre A, Waget A, Burcelin R, Lière P, et al. Prevention of obesity and insulin resistance by estrogens requires ERα activation function-2 (ERαAF-2), whereas ERαAF-1 is dispensable. *Diabetes.* 2013;62(12):4098-108.

77. Savage DB. Mouse models of inherited lipodystrophy. *Dis. Model. Mech.* 2009;2(11-12):554-62.

78. Agrawal S, Luan J, Cummings BB, Weiss EJ, Wareham NJ, and Khera AV. Relationship of Fat Mass Ratio, a Biomarker for Lipodystrophy, With Cardiometabolic Traits. *Diabetes.* 2024;73(7):1099-111.

79. Latchman DS. Transcription-Factor Mutations and Disease. *N. Engl. J. Med.* 1996;334(1):28-33.

80. Barroso I, Gurnell M, Crowley VEF, Agostini M, Schwabe JW, Soos MA, et al. Dominant negative mutations in human PPARγ associated with severe insulin resistance, diabetes mellitus and hypertension. *Nature.* 1999;402(6764):880-3.

81. Pfäffle RW, DiMattia GE, Parks JS, Brown MR, Wit JM, Jansen M, et al. Mutation of the POU-specific domain of Pit-1 and hypopituitarism without pituitary hypoplasia. *Science.* 1992;257(5073):1118-21.

82. Baniahmad A, Tsai SY, O'Malley BW, and Tsai MJ. Kindred S thyroid hormone receptor is an active and constitutive silencer and a repressor for thyroid hormone and retinoic acid responses. *Proc. Natl. Acad. Sci. U. S. A.* 1992;89(22):10633-7.

83. Kaneshige A, Bai L, Wang M, McEachern D, Meagher JL, Xu R, et al. A selective small-molecule STAT5 PROTAC degrader capable of achieving tumor regression in vivo. *Nat. Chem. Biol.* 2023;19(6):703-11.

84. Havens MA, and Hastings ML. Splice-switching antisense oligonucleotides as therapeutic drugs. *Nucleic Acids Res.* 2016;44(14):6549-63.

85. Wang C-H, Lundh M, Fu A, Kriszt R, Huang TL, Lynes MD, et al. CRISPR-engineered human brown-like adipocytes prevent diet-induced obesity and ameliorate metabolic syndrome in mice. *Sci. Transl. Med.* 2020;12(558):eaaz8664.

Figure 1. Identification of EBF2 p.E165X variant and in vitro functional screening.

(A) Patient with atypical partial lipodystrophy showing altered fat distribution, dorsal neck fat pad with acanthosis (arrow), and prominent veins in legs (arrows). (B) Whole-body DEXA "fat shadow." (C) H&E and Masson's trichrome of liver, kidney, and subcutaneous WAT (abdomen, neck, thigh); collagen in blue. (D) Sanger sequencing showing G>T substitution. (E) 3T3-L1 cells transduced with empty, full-length EBF2, or truncated EBF2 (1–164); GFP (green), BODIPY (red), DAPI (blue). (F) Luciferase reporter assay in HEK cells (n=3). Scale bar, 100 μm (C, E). One-way ANOVA with Tukey's test, ****$p<0.0001$ (F). Data are mean ± SEM. Each dot represents a biological replicate. See also Supplemental Figure 1.

Figure 2. *EBF2* p.E165X impairs postnatal adipose tissue expansion and remodeling.

(A and B) H&E and Masson's trichrome of IWAT (A) and GWAT (B) from 16-week-old mice (n=4). Collagen (blue); stromal clusters (arrows). (C) Quantification of IWAT fibrosis (%) (n=3–4). (D) RT-qPCR of adipogenic genes in IWAT (n=4–6). (E) IWAT immunofluorescence of CD34 and fibronectin (red); DAPI (blue). Scale bar, 100 μm. Student's t-test, *$p<0.05$, **$p<0.01$ (D). Two-way ANOVA with Tukey's test, **$p<0.01$, ***$p<0.001$ (C). Data are mean ± SEM. Each dot represents a mouse (D) or an HPF (C). See also Supplemental Figures 2 and 3.

Figure 3. EBF2 p.E165X disrupts HFD-induced adipose remodeling.

8-week-old mice (n=11–15 per group) were fed HFD for 2 months. (A, B) Body weight at baseline and after HFD. (C) Food intake at week 8 (n=8/group). (D, E) Fat and lean mass by NMR (n=8/group). (F, G) Serum leptin and adiponectin (n=6–8/group). (H, I) H&E and trichrome of IWAT and GWAT showing collagen (blue) and immune infiltrates (arrows). (J, K) Quantification of adipocyte area and number in IWAT (J) and GWAT (K) (n=3–4/group). (L) IWAT and GWAT fibrosis (%) (n=3–4/group). Scale bar, 100 μm. Two-way ANOVA or t-test, *$p<0.05$, **$p<0.01$, ***$p<0.001$, ****$p<0.0001$. Data are mean ± SEM. Each dot = mouse (A–G) or HPF (J–L). See also Supplemental Figures 4–6.

Figure 4. EBF2 p.E165X worsens HFD-associated metabolic phenotypes.

(A) Serum glucose after 8 weeks of HFD (n=6–8). (B, C) IPGTT and AUC (n=8). (D) Masson's trichrome of liver. (E) %BAT weight (n=8–15). Scale bar, 100 μm. Two-way ANOVA or t-test, *p<0.05, **p<0.01, ns not significant. Data are mean ± SEM. Each dot = mouse. See also Supplemental Figures 4–6.

Figure 5. EBF2 p.E165X alters IWAT identity.

(A) Volcano plot of differentially expressed genes in 4-week-old male IWAT (n=3/group). (B) Downregulated pathways (Hallmark, GO). (C, D) Heat maps of genes involved in oxidative phosphorylation and fatty acid metabolism. (E) TEM of IWAT with mitochondria (arrows) and lipid droplets (LD). (F–H) Quantification of mitochondrial area, electron density, and distance to LD. Scale bar, 1 μm (main), 500 nm (insets). *p<0.05, **p<0.01.

Figure 6. The EBF2 variant impairs adipocyte differentiation in a cell-autonomous, dominant-negative manner.

(A) Allele-specific RT-qPCR of IWAT (n=3–5). (B) Differentiated IWAT SVF from $Ebf2^{+/+}$ and $Ebf2^{E165X/+}$; BODIPY (green), DAPI (blue). (C) Quantification of lipid accumulation (n=6). (D, E) Expression of adipogenic genes and Ebf family members in SVF before/after differentiation (n=5). (F) Effects of truncated/full-length EBF2 and shRNAs in SVF. (G, H) Quantification of lipid accumulation and gene expression (n=3). Scale bar, 100 μm. One-way or two-way ANOVA with Tukey's test. *p<0.05, **p<0.01, ***p<0.001, ****p<0.0001. Data are mean ± SEM. See also Supplemental Figures 1 and 7.

Figure 7. Effects of the *EBF2* variant on human adipocytes and patient WAT.

(A) Human SQ preadipocytes transduced with control, full-length, or truncated *EBF2*; BODIPY (red), GFP (green), DAPI (blue). (B) Quantification (n=2). (C) Venn diagram of RNA-seq differentially expressed genes. (D, E) Heat maps of ECM and cytokine receptor genes. (F, G)

CyTOF of patient neck WAT showing DNA, collagen I, CD34, CD15, CD11c, CD68. (H, I) Immunofluorescence of patient/control WAT depots. Scale bar, 100 µm. One-way ANOVA with Tukey’s test, $^{**}p<0.01$, $^{***}p<0.001$. Data are mean ± SEM. Each dot presents a single image.

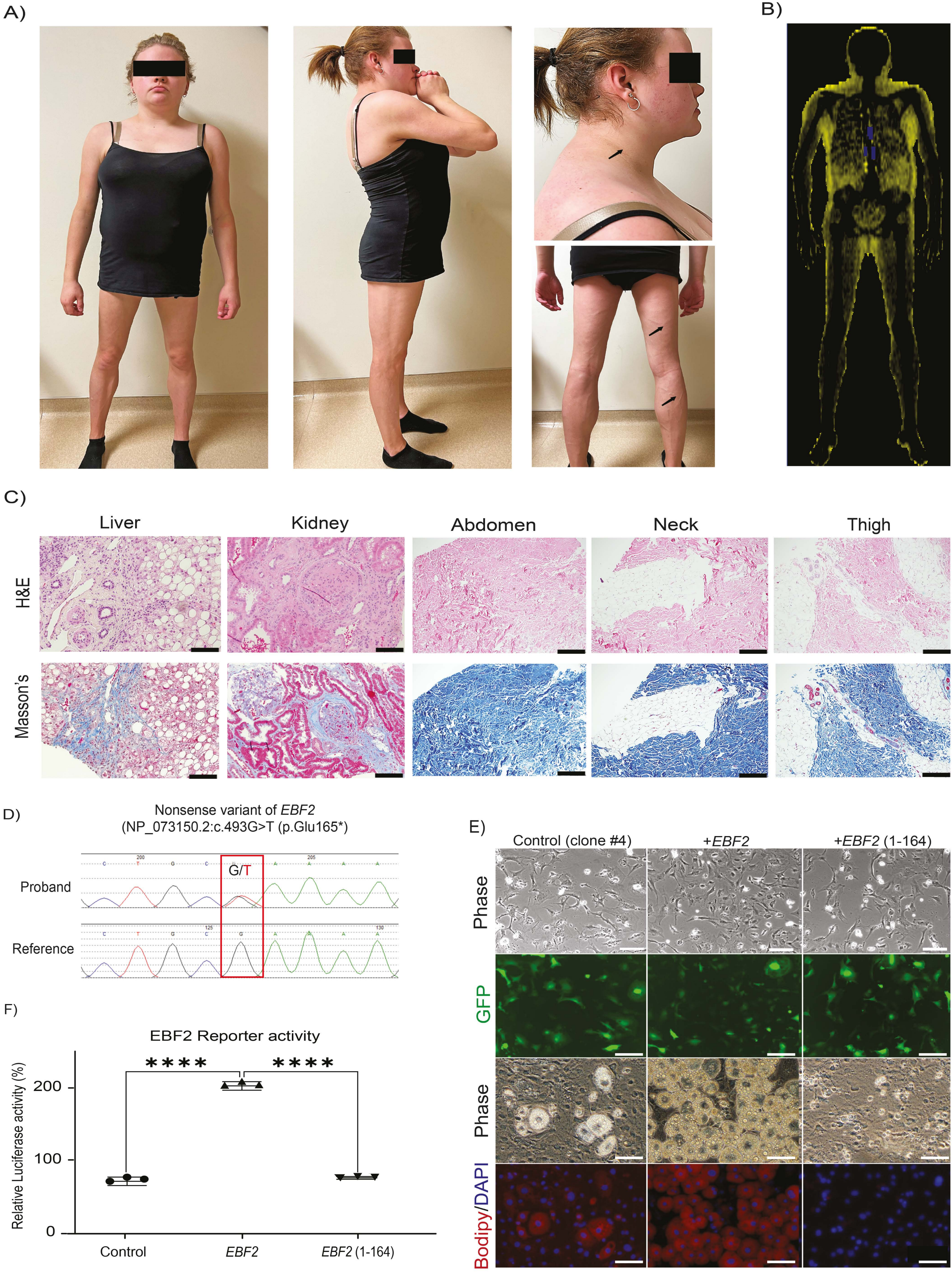
A)
B)
C)
Liver
Kidney
Abdomen
Neck
Thigh
H&E
Masson's
D)
Nonsense variant of EBF2
(NP_073150.2:c.493G>T (p.Glu165*))
Proband
Reference
G/T
200
205
125
130
E)
Control (clone #4)
+EBF2
+EBF2 (1-164)
Phase
GFP
Phase
Bodipy/DAPI
F)
EBF2 Reporter activity
Relative Luciferase activity (%)
0
100
200
****
****
Control
EBF2
EBF2 (1-164)

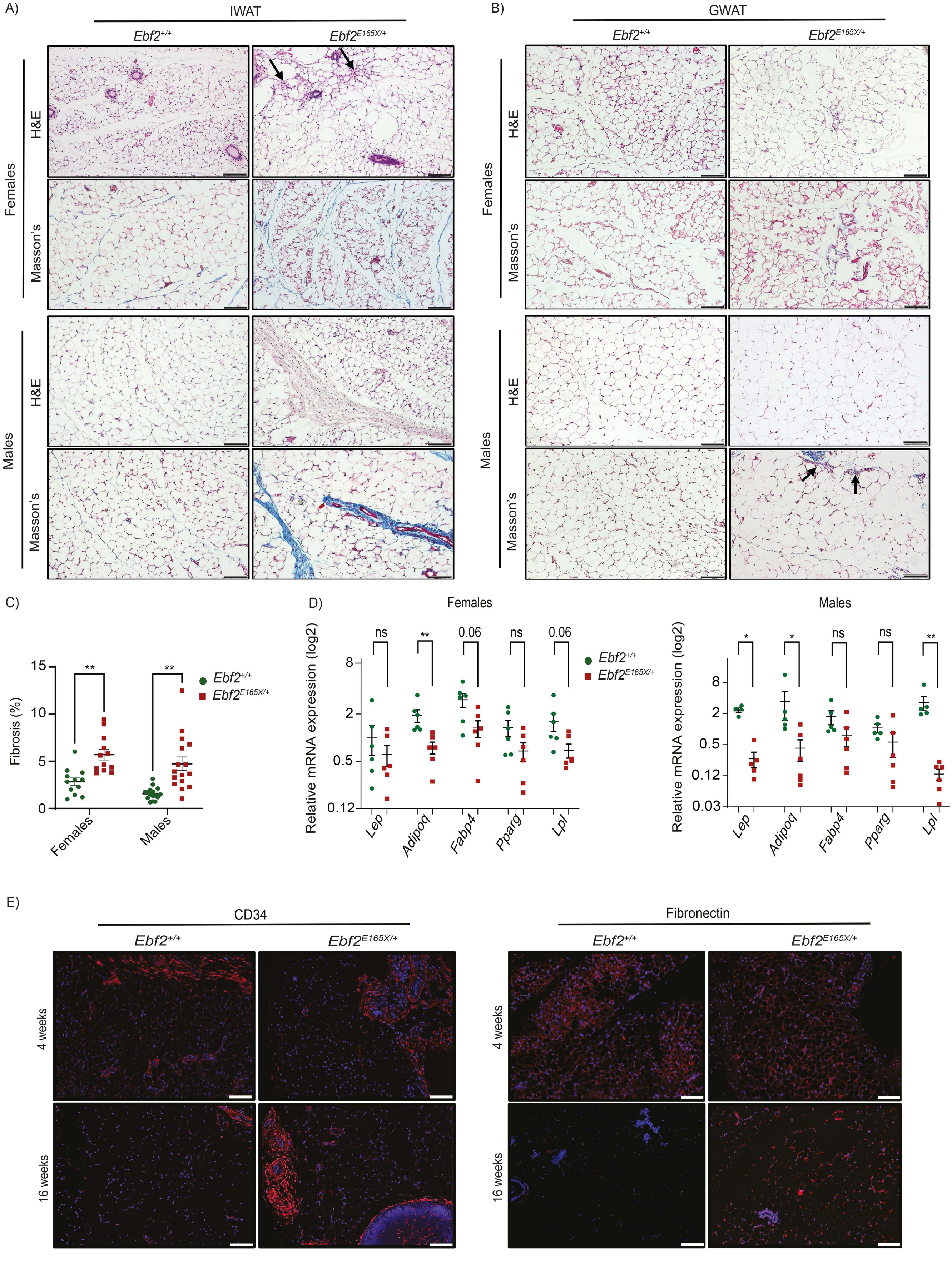
A)
IWAT
Ebf2+/+
Ebf2E165X/+
Females
H&E
Masson's
Males
H&E
Masson's
B)
GWAT
Ebf2+/+
Ebf2E165X/+
Females
H&E
Masson's
Males
H&E
Masson's
C)
Fibrosis (%)
15
10
5
0
**
**
Females
Males
Ebf2+/+
Ebf2E165X/+
D)
Females
Relative mRNA expression (log2)
8
2
0.5
0.12
ns
**
0.06
ns
0.06
Lep
Adipoq
Fabp4
Pparg
Lpl
Ebf2+/+
Ebf2E165X/+
Males
Relative mRNA expression (log2)
8
2
0.5
0.12
0.03
*
*
ns
ns
**
Lep
Adipoq
Fabp4
Pparg
Lpl
E)
CD34
Ebf2+/+
Ebf2E165X/+
4 weeks
16 weeks
Fibronectin
Ebf2+/+
Ebf2E165X/+
4 weeks
16 weeks

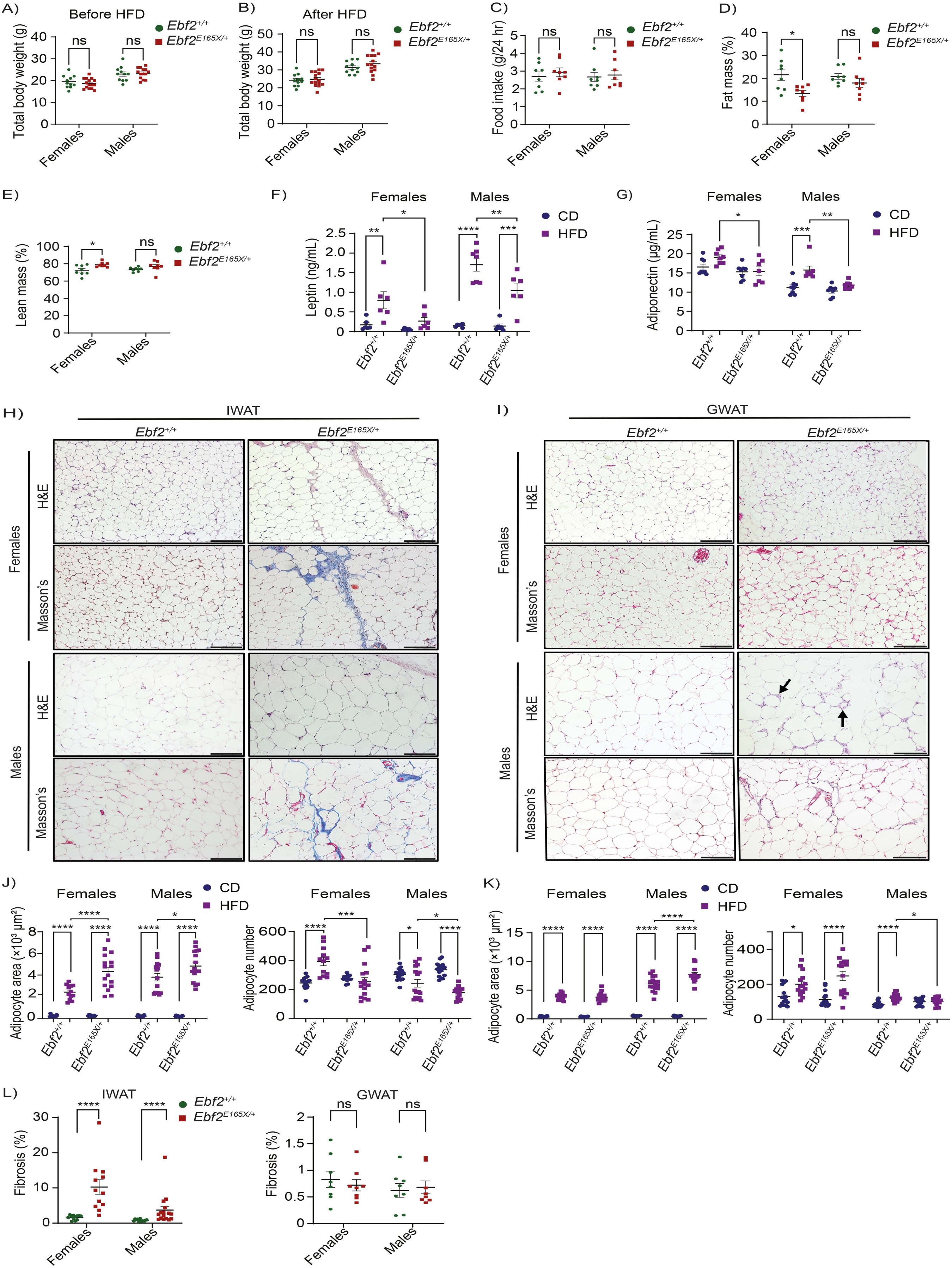
A)
Before HFD
Total body weight (g)
ns
ns
Females
Males
Ebf2+/+
Ebf2E165X/+
B)
After HFD
Total body weight (g)
ns
ns
C)
Food intake (g/24 hr)
ns
ns
D)
Fat mass (%)
*
ns
E)
Lean mass (%)
*
ns
F)
Females
Males
Leptin (ng/mL)
CD
HFD
**
*
****
**
***
G)
Adiponectin (µg/mL)
*
***
**
H)
IWAT
Ebf2+/+
Ebf2E165X/+
Females
Males
H&E
Masson's
I)
GWAT
Ebf2+/+
Ebf2E165X/+
Females
Males
H&E
Masson's
J)
Adipocyte area (×10³ µm²)
Adipocyte number
****
*
***
K)
Adipocyte area (×10³ µm²)
Adipocyte number
L)
IWAT
GWAT
Fibrosis (%)
****
ns

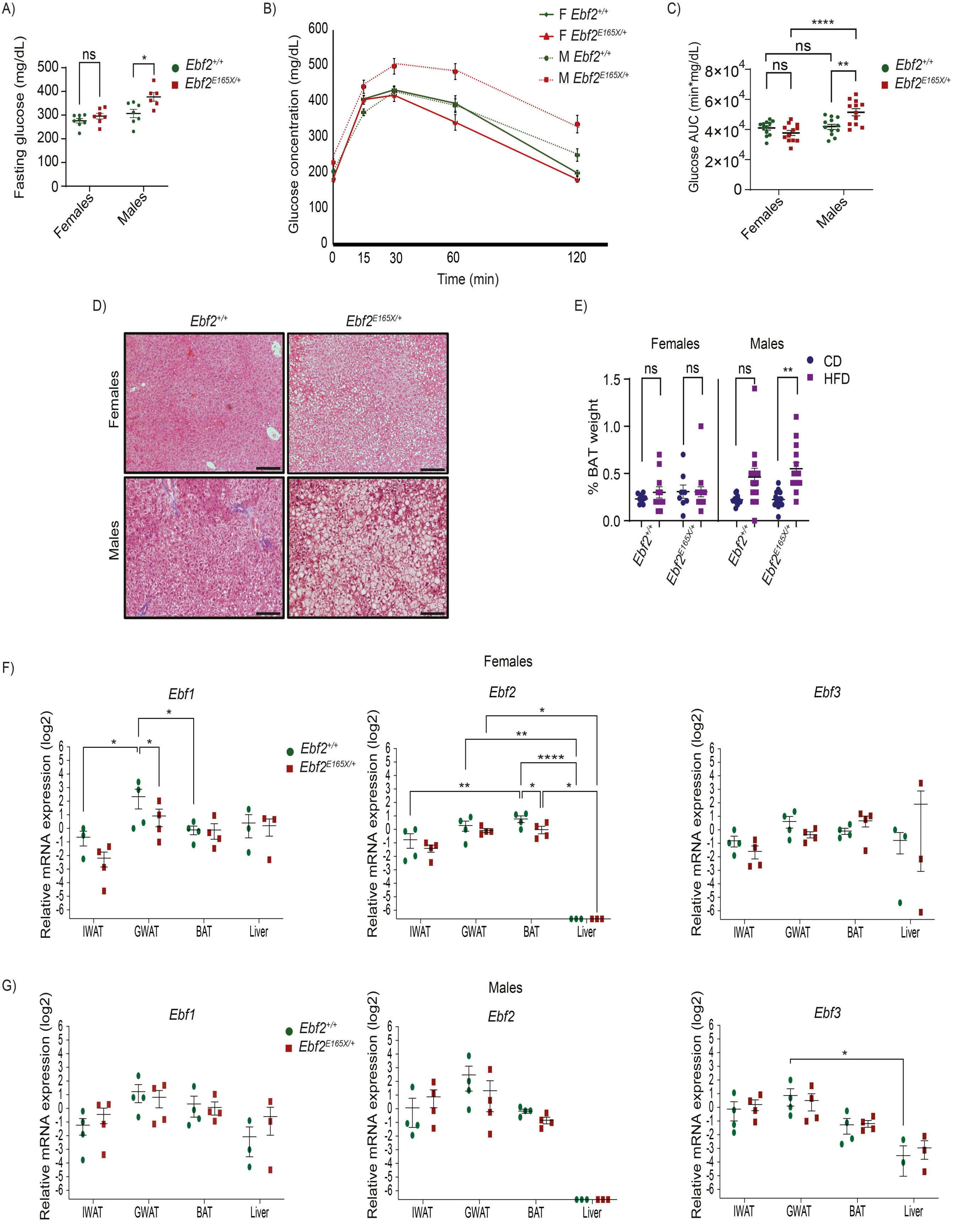
A)
Fasting glucose (mg/dL)
ns
*
Ebf2+/+
Ebf2E165X/+
Females
Males
B)
Glucose concentration (mg/dL)
Time (min)
F Ebf2+/+
F Ebf2E165X/+
M Ebf2+/+
M Ebf2E165X/+
C)
Glucose AUC (min*mg/dL)
****
ns
ns
**
Ebf2+/+
Ebf2E165X/+
Females
Males
D)
Ebf2+/+
Ebf2E165X/+
Females
Males
E)
Females
Males
% BAT weight
ns
ns
ns
**
CD
HFD
Ebf2+/+
Ebf2E165X/+
Ebf2+/+
Ebf2E165X/+
F)
Females
Ebf1
Ebf2
Ebf3
Relative mRNA expression (log2)
Ebf2+/+
Ebf2E165X/+
IWAT
GWAT
BAT
Liver
*
**
****
G)
Males
Ebf1
Ebf2
Ebf3
Relative mRNA expression (log2)
Ebf2+/+
Ebf2E165X/+
IWAT
GWAT
BAT
Liver
*

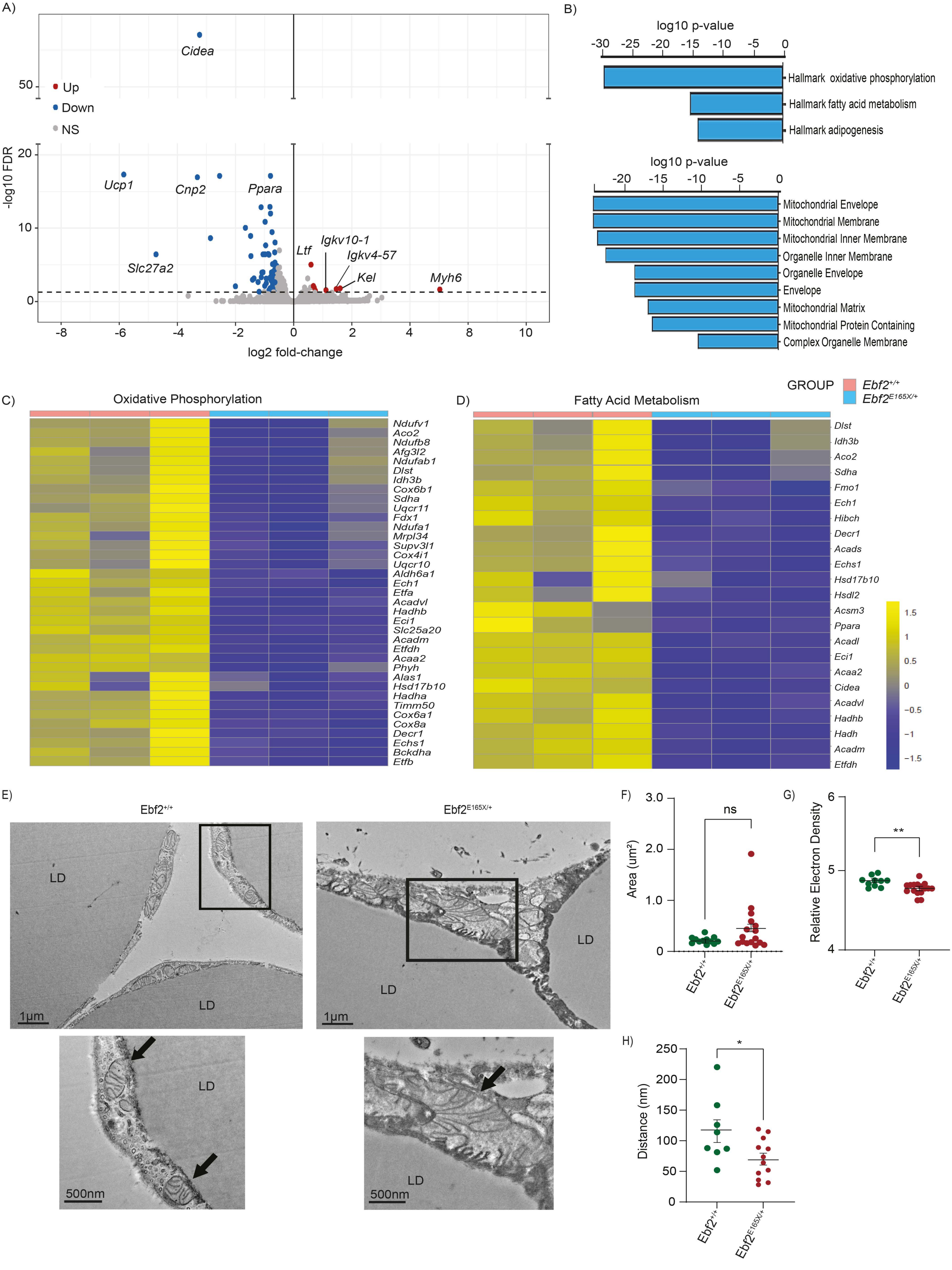
A)
Cidea
Up
Down
NS
50
-log10 FDR
20
10
0
Ucp1
Cnp2
Ppara
Slc27a2
Ltf
Igkv10-1
Igkv4-57
Kel
Myh6
-8
-6
-4
-2
0
2
4
8
10
log2 fold-change
B)
log10 p-value
-30 -25 -20 -15 -10 -5 0
Hallmark oxidative phosphorylation
Hallmark fatty acid metabolism
Hallmark adipogenesis
log10 p-value
-20 -15 -10 -5 0
Mitochondrial Envelope
Mitochondrial Membrane
Mitochondrial Inner Membrane
Organelle Inner Membrane
Organelle Envelope
Envelope
Mitochondrial Matrix
Mitochondrial Protein Containing
Complex Organelle Membrane
C)
Oxidative Phosphorylation
Ndufv1
Aco2
Ndufb8
Afg3l2
Ndufab1
Dlst
Idh3b
Cox6b1
Sdha
Uqcr11
Fdx1
Ndufa1
Mrpl34
Supv3l1
Cox4i1
Uqcr10
Aldh6a1
Ech1
Etfa
Acadvl
Hadhb
Eci1
Slc25a20
Acadm
Etfdh
Acaa2
Phyh
Alas1
Hsd17b10
Hadha
Timm50
Cox6a1
Cox8a
Decr1
Echs1
Bckdha
Etfb
D)
Fatty Acid Metabolism
GROUP
Ebf2+/+
Ebf2E165X/+
Dlst
Idh3b
Aco2
Sdha
Fmo1
Ech1
Hibch
Decr1
Acads
Echs1
Hsd17b10
Hsdl2
Acsm3
Ppara
Acadl
Eci1
Acaa2
Cidea
Acadvl
Hadhb
Hadh
Acadm
Etfdh
1.5
1
0.5
0
−0.5
−1
−1.5
E)
Ebf2+/+
Ebf2E165X/+
LD
LD
LD
LD
LD
1μm
1μm
LD
LD
500nm
500nm
F)
3.0
2.0
1.0
0
Area (um²)
ns
Ebf2+/+
Ebf2E165X/+
G)
6
5
4
Relative Electron Density
**
Ebf2+/+
Ebf2E165X/+
H)
250
200
150
100
50
0
Distance (nm)
*
Ebf2+/+
Ebf2E165X/+

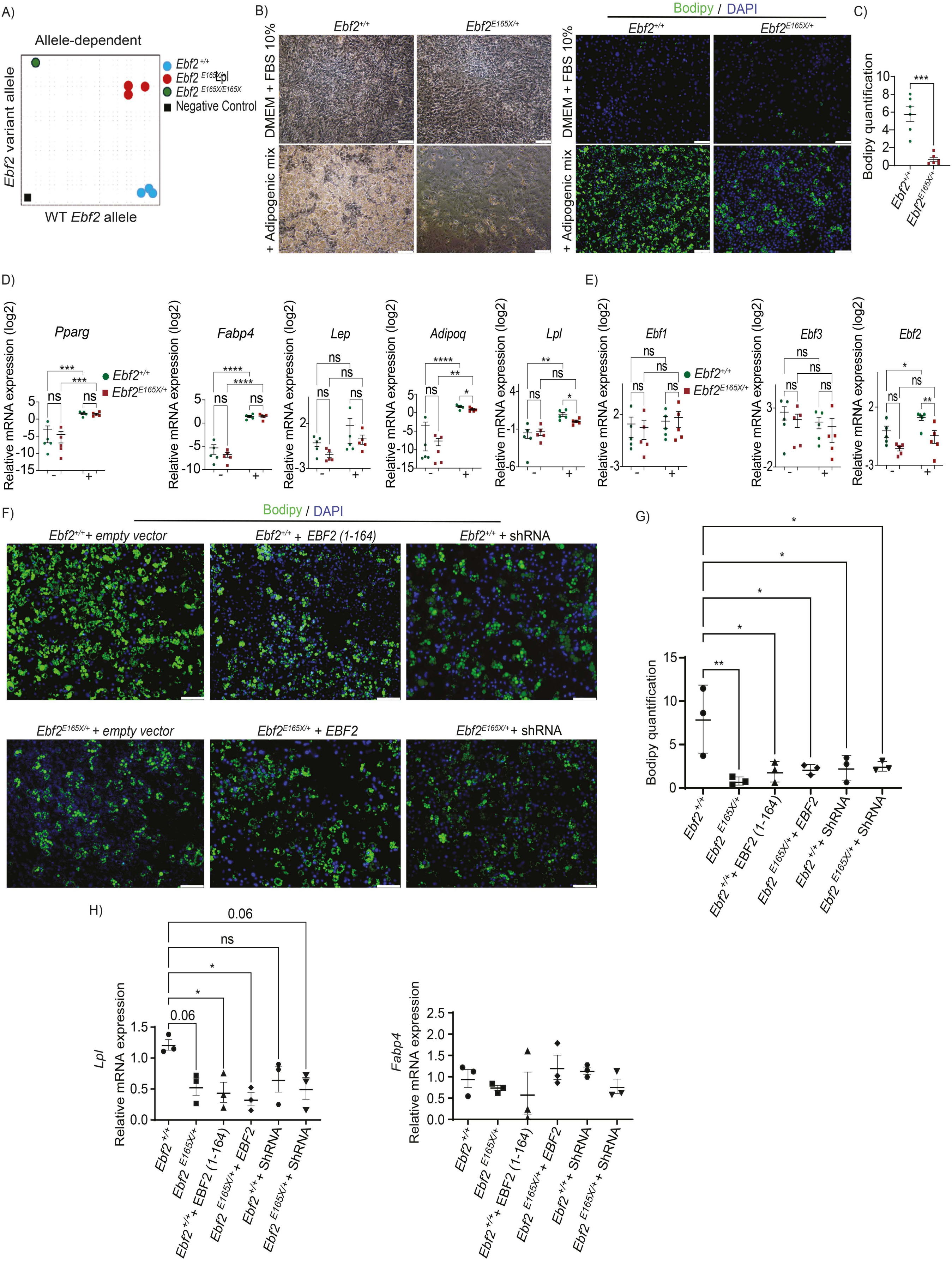
A)
Allele-dependent
Ebf2 variant allele
WT Ebf2 allele
Ebf2 +/+
Ebf2 E165X/+
Ebf2 E165X/E165X
Negative Control
B)
Ebf2+/+
Ebf2E165X/+
DMEM + FBS 10%
+ Adipogenic mix
Bodipy / DAPI
C)
Bodipy quantification
***
Ebf2+/+
Ebf2E165X/+
D)
Relative mRNA expression (log2)
Pparg
Fabp4
Lep
Adipoq
Lpl
Ebf2+/+
Ebf2E165X/+
ns
*
**
***
****
-
+
E)
Ebf1
Ebf3
Ebf2
F)
Bodipy / DAPI
Ebf2+/+ + empty vector
Ebf2+/+ + EBF2 (1-164)
Ebf2+/+ + shRNA
Ebf2E165X/+ + empty vector
Ebf2E165X/+ + EBF2
Ebf2E165X/+ + shRNA
G)
Bodipy quantification
Ebf2 +/+
Ebf2 E165X/+
Ebf2 +/+ + EBF2 (1-164)
Ebf2 E165X/+ + EBF2
Ebf2 +/+ + ShRNA
Ebf2 E165X/+ + ShRNA
H)
Lpl
Relative mRNA expression
0.06
ns
Fabp4

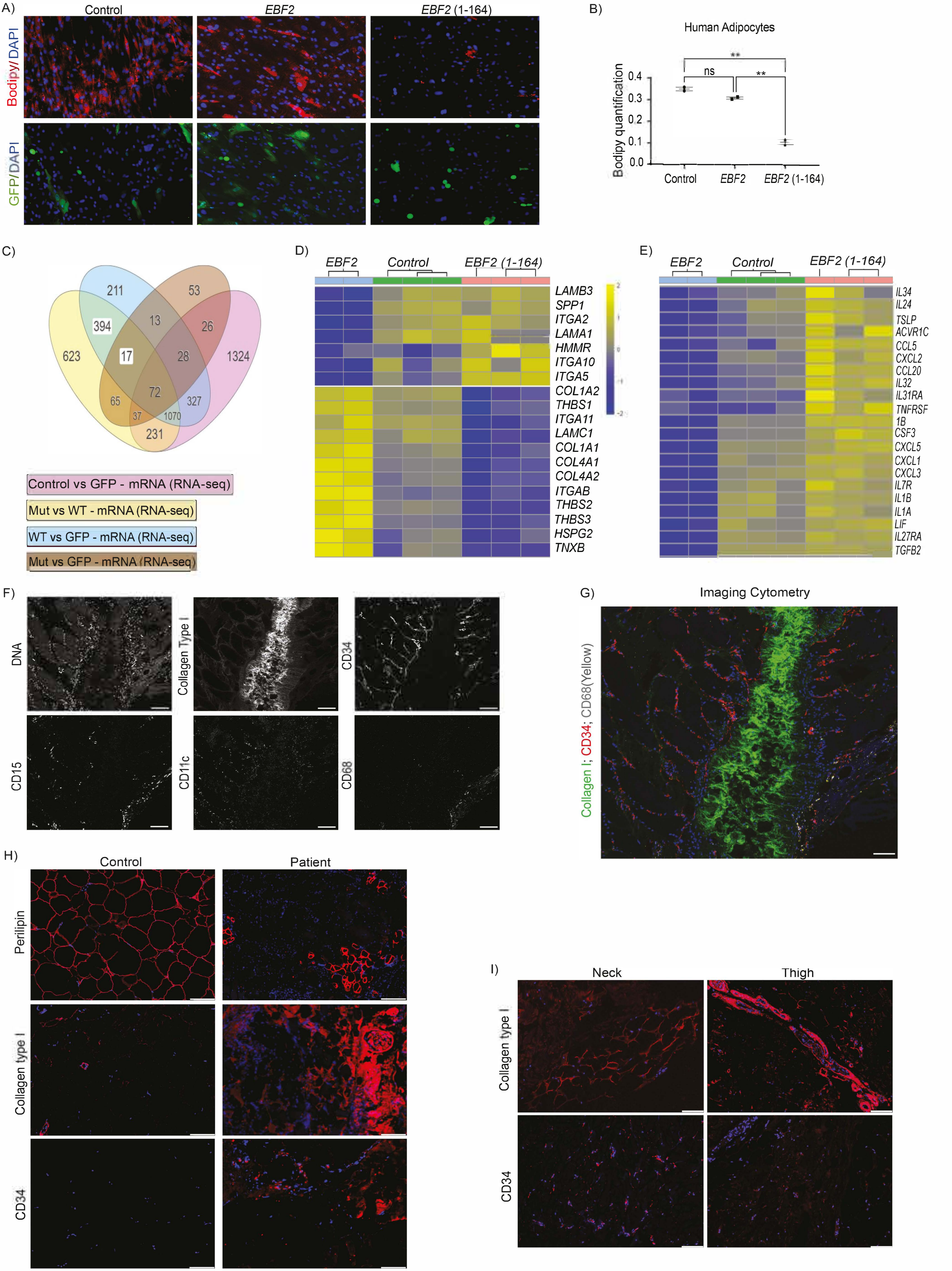
A)
Control
EBF2
EBF2 (1-164)
Bodipy/ DAPI
GFP/DAPI
B)
Human Adipocytes
Bodipy quantification
0.4
0.3
0.2
0.1
0.0
ns
**
**
Control
EBF2
EBF2 (1-164)
C)
211
53
394
13
26
623
17
28
1324
72
65
327
37
1070
231
Control vs GFP - mRNA (RNA-seq)
Mut vs WT - mRNA (RNA-seq)
WT vs GFP - mRNA (RNA-seq)
Mut vs GFP - mRNA (RNA-seq)
D)
EBF2
Control
EBF2 (1-164)
LAMB3
SPP1
ITGA2
LAMA1
HMMR
ITGA10
ITGA5
COL1A2
THBS1
ITGA11
LAMC1
COL1A1
COL4A1
COL4A2
ITGAB
THBS2
THBS3
HSPG2
TNXB
2
1
0
-1
-2
E)
EBF2
Control
EBF2 (1-164)
IL34
IL24
TSLP
ACVR1C
CCL5
CXCL2
CCL20
IL32
IL31RA
TNFRSF
1B
CSF3
CXCL5
CXCL1
CXCL3
IL7R
IL1B
IL1A
LIF
IL27RA
TGFB2
F)
DNA
Collagen Type I
CD34
CD15
CD11c
CD68
G)
Imaging Cytometry
Collagen I; CD34; CD68(Yellow)
H)
Control
Patient
Perilipin
Collagen type I
CD34
I)
Neck
Thigh
Collagen type I
CD34